

Protein complexes containing CYFIP/Sra/PIR121 coordinate Arf1 and Rac1 signalling during clathrin–AP-1-coated carrier biogenesis at the TGN

Mihaela Anitei¹, Christoph Stange¹, Irina Parshina¹, Thorsten Baust^{1,2}, Annette Schenck³, Graça Raposo^{4,5,6}, Tomas Kirchhausen² and Bernard Hoflack^{1*}

Actin dynamics is a tightly regulated process involved in various cellular events including biogenesis of clathrin-coated, AP-1 (adaptor protein 1)-coated transport carriers connecting the trans-Golgi network (TGN) and the endocytic pathway. However, the mechanisms coordinating coat assembly, membrane and actin remodelling during post-TGN transport remain poorly understood. Here we show that the Arf1 (ADP-ribosylation factor 1) GTPase synchronizes the TGN association of clathrin–AP-1 coats and protein complexes comprising CYFIP (cytoplasmic fragile-X mental retardation interacting protein; Sra, PIR121), a clathrin heavy chain binding protein associated with mental retardation. The Rac1 GTPase and its exchange factor β -PIX (PAK-interacting exchange factor) activate these complexes, allowing N-WASP-dependent and Arp2/3-dependent actin polymerization towards membranes, thus promoting tubule formation. These phenomena can be recapitulated with synthetic membranes. This protein-network-based mechanism facilitates the sequential coordination of Arf1-dependent membrane priming, through the recruitment of coats and CYFIP-containing complexes, and of Rac1-dependent actin polymerization, and provides complementary but independent levels of regulation during early stages of clathrin–AP1-coated carrier biogenesis.

In mammalian cells, clathrin and the AP-1 adaptor mediate the trafficking of specific cargoes, including the mannose-6-phosphate receptors (MPRs) and their bound lysosomal enzymes, from the TGN to the endosomal system^{1–3}. The small Arf1 GTPase has a central function in clathrin–AP-1 coat recruitment onto membranes. Arf1•GTP activates phosphatidylinositol (PI)-4-OH kinases^{4,5} and, together with PI(4)P and sorting signals present in cytoplasmic domains of selected cargoes, binds AP-1 (refs 6–8), leading to coat recruitment on to membranes followed by membrane remodelling and transport carrier formation. Actin dynamics also regulates post-Golgi transport^{9,10} while maintaining Golgi integrity in non-dividing cells¹¹ and controlling Golgi dynamics during cell division¹². The actin cytoskeleton and its regulators HIP1R (huntingtin-interacting protein 1-related protein)¹³ and cortactin¹⁴ are involved in the biogenesis of both clathrin–AP-1-coated and endocytic, clathrin–AP-2-coated vesicles^{15–17}. It is unclear whether actin dynamics at these different locations or during the cell cycle requires the same protein networks and the same regulatory mechanisms.

A key regulator of actin nucleation is the Arp2/3 complex¹⁸. Its activity at various cellular locations depends on Rho GTPase-regulated factors¹⁹ comprising WASP, N-WASP (Wiskott–Aldrich syndrome proteins), WAVE1–WAVE3 (WASP family Verprolin-homologous proteins) and

WHAMM (WASP homolog associated with actin, membranes and microtubules)²⁰. These related WAVE and WASP proteins associate with a complex formed from Abi1 (Abelson-interacting protein), NAP1 (Nck-associated protein or p125^{NAP1}), HSPC 300 (BRICK) and CYFIP1 and CYFIP2 (also known as Sra1 and PIR121, respectively)¹⁹, which interact with the fragile-X mental retardation protein²¹. This protein complex regulates Rac1-dependent WAVE2 function at cellular leading edges during cell motility^{22–25}. Abi1 also binds N-WASP and has a function in endocytosis after Cdc42-mediated activation^{26,27}. Thus, the activity of this CYFIP-containing complex may require the combinatorial use of different proteins to promote actin polymerization at various locations.

Although it is clear that membrane and actin remodelling are intimately linked, the mechanisms coordinating these processes remain poorly understood. We have previously identified, among the 40 proteins associated *in vitro* with clathrin–AP-1-coated membranes, the Arp2/3 complex, WAVE proteins and a protein complex containing CYFIP1, CYFIP2, Abi1, Abi2 and NAP1 (ref. 8). Here we show the functional significance of Arf1, clathrin, CYFIP1, CYFIP2, N-WASP, WASP, Rac1 and its exchange factor β -PIX (ARHGEF7) as key components of the different cellular machines shaping clathrin–AP-1-coated carriers and regulating their biogenesis.

¹Biotechnology Center, Dresden University of Technology, Tatzberg 47-51, 01307 Dresden, Germany. ²Harvard Medical School/CBRI, W. Alpert Building Room 128, 200 Longwood Avenue, Boston, Massachusetts 02115, USA. ³Nijmegen Centre for Molecular Life Sciences, Donders Institute for Brain, Cognition and Behaviour & Radboud University Nijmegen Medical Center, Department of Human Genetics, Geert Grooteplein 10, 6525 GA Nijmegen, The Netherlands. ⁴Institut Curie, Centre de Recherche, ⁵CNRS, UMR144, ⁶Cell and Tissue Imaging facility (IBiSA), Paris, F-75248, France.

*Correspondence should be addressed to B.H. (e-mail: bernard.hoflack@biotec.tu-dresden.de)

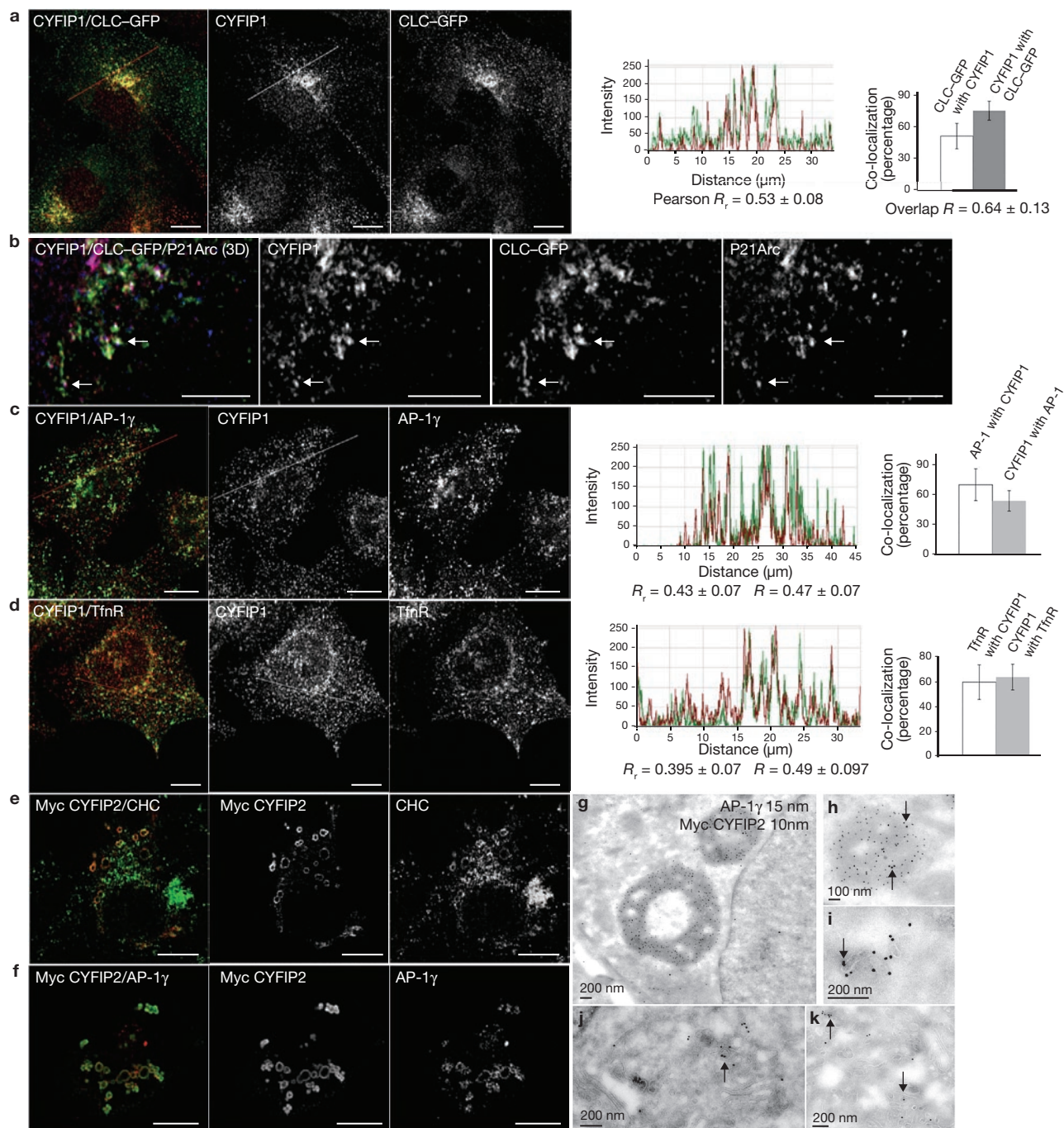


Figure 1 Localization of CYFIP1 and CYFIP2. **(a, b)** BSC-1 cells stably expressing clathrin light chain coupled to enhanced green fluorescent protein (CLC-EGFP) were labelled with antibodies against CYFIP1 (red) **(a, b)** and p21Arc (blue) **(b)**. **(c, d)** HeLa cells were labelled with antibodies against CYFIP1 (red) and AP-1 γ (green) **(c)** or transferrin receptor (green) **(d)**. **(e, f)** HeLa cells transiently expressing Myc-tagged CYFIP2 were labelled with antibodies against Myc, CHC (green) **(e)** or AP-1 γ (red) **(f)**. Co-localization was analysed and quantified with Volocity 5.2 software. R represents the overlap

coefficients, and R_r the Pearson correlation coefficients. Data are shown as means \pm s.d. (in each case, 20–25 cells from $n = 3$ different experiments). Scale bars, 10 μm **(a, c–f)**, 5 μm **(b)**. **(g–k)** HeLa cells transiently expressing Myc-tagged CYFIP2 were processed for electron microscopy. Thawed cryosections were co-labelled with anti-AP-1 antibodies (15-nm gold particles) and anti-Myc antibodies (10-nm gold particles). Arrows indicate AP-1 present on Myc-tagged CYFIP2 enlarged intracellular structures **(g, h)** and AP-1 and CYFIP2 co-localization on intracellular membranes **(i–k)**.

RESULTS

Subcellular distribution of CYFIP1 and CYFIP2

We first analysed the cellular distribution of CYFIP1 and CYFIP2, which are believed to form heterodimers²⁸. Statistical image analysis indicated that half of the endogenous CYFIP1 was detected in the perinuclear region on

clathrin-AP-1-positive structures (Fig. 1a–c) containing part of the transferrin receptor (TfnR) (Fig. 1d). These structures also contained a transmembrane protein made of green fluorescent protein (GFP) fused to the transmembrane and cytoplasmic domains of the cation-independent MPR (here referred to as the GFP-MPR tail), which mostly localizes to the TGN

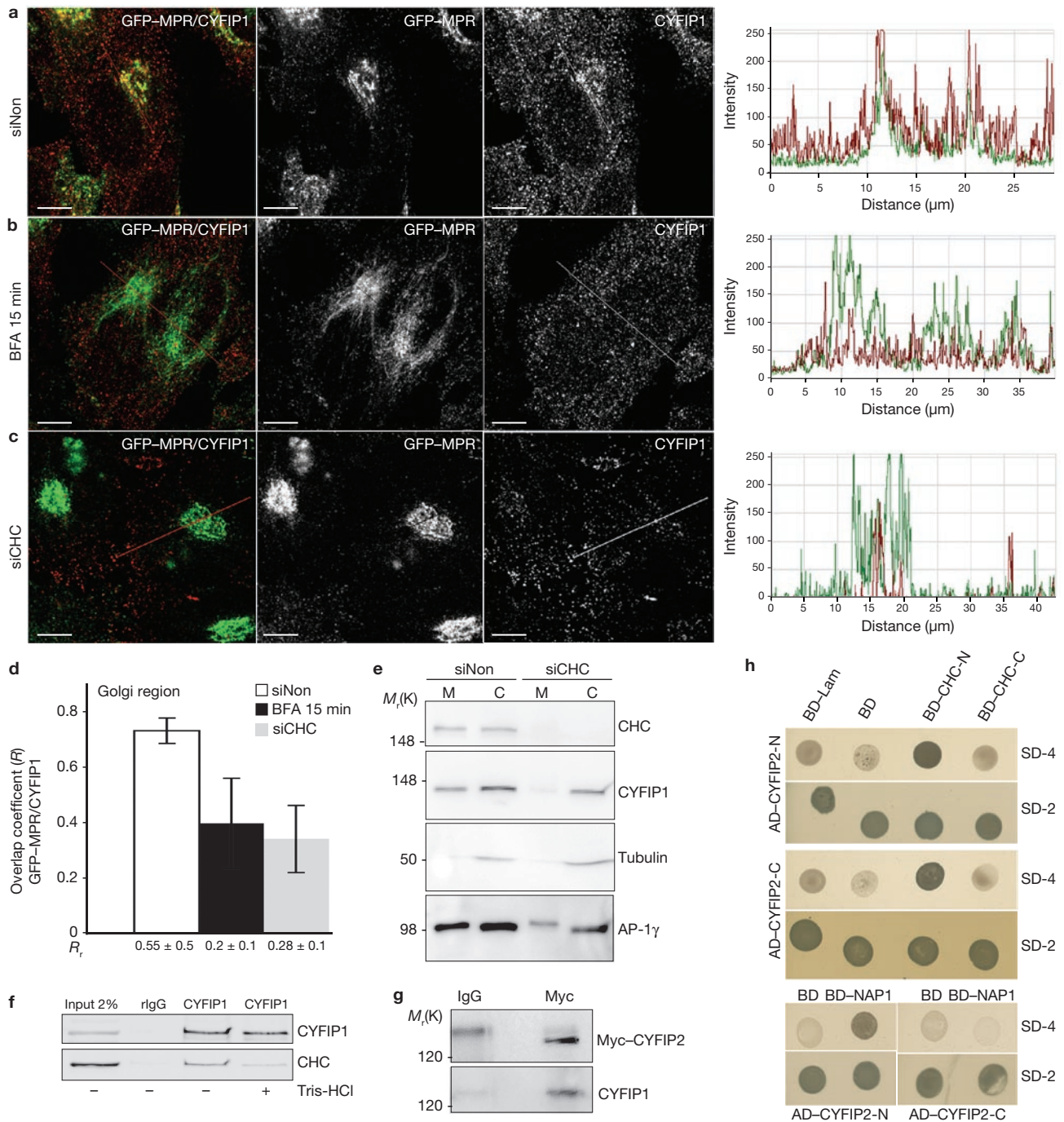


Figure 2 CYFIP1 and CYFIP2 interact with CHC, and CYFIP1 recruitment to the TGN is regulated by Arf1. **(a–d)** HeLa cells stably expressing GFP-MPR were treated with control siRNA (siNon; **a**) or siRNAs to deplete CHC (siCHC; **c**) or incubated with 5 $\mu\text{g ml}^{-1}$ BFA for 15 min (**b**). Cells were then labelled with anti-CYFIP1 (red), and the overlap (R) and Pearson correlation (R_i) coefficients between GFP-MPR and CYFIP1 in the TGN region were quantified for each condition (**d**) (20 cells from $n = 3$ independent experiments were analysed per condition; data are shown as means \pm s.d.). Scale bars, 10 μm . **(e)** The membrane (M) and cytosolic (C) fractions of HeLa cells incubated either with siNon or with siCHC were analysed by western blotting ($n = 3$ independent experiments). **(f)** COS-7 cell lysates were incubated with anti-CYFIP1 or with control pre-immune rabbit IgG. Beads were washed with buffer with or without 0.5 M Tris-HCl (pH 7.4), which induces clathrin cage depolymerization. The presence of CHC and CYFIP1 in the immunoprecipitates was determined by western blotting with the corresponding antibodies. CHC was co-immunoprecipitated with

CYFIP1 only in the absence of TrisHCl ($n = 3$ independent experiments). **(g)** Lysates of HeLa cells transiently expressing Myc-tagged CYFIP2 were incubated with anti-Myc or control mouse IgGs, and the immunoprecipitates were analysed by western blotting. Full scans of all gels are shown in Supplementary Information, Fig. S9. **(h)** The N-terminal (AD-CYFIP2-N, residues 2–623) and C-terminal (AD-CYFIP2-C, residues 674–1299) domains of CYFIP2 were expressed as fusions with GAL4AD (pGADT7). The N-terminal (BD-CLC-N, residues 1–690) and C-terminal (BD-CLC-C, residues 821–1679) halves of clathrin heavy chain, as well as full-length NAP1. **(i)** were fused to the DNA-BD (pGBKT7) and co-expressed with the GAL4AD-containing plasmids (AD, activation domain; BD, binding domain). Interactions were detected by growth on agar plates lacking leucine and tryptophane (SD-2) or lacking adenine, histidine, leucine and tryptophan (SD-4). Plasmids expressing either fusion of lamin C to the DNA-BD (BD-Lam) or DNA-BD alone (BD) were used as negative controls. $n = 3$ independent experiments.

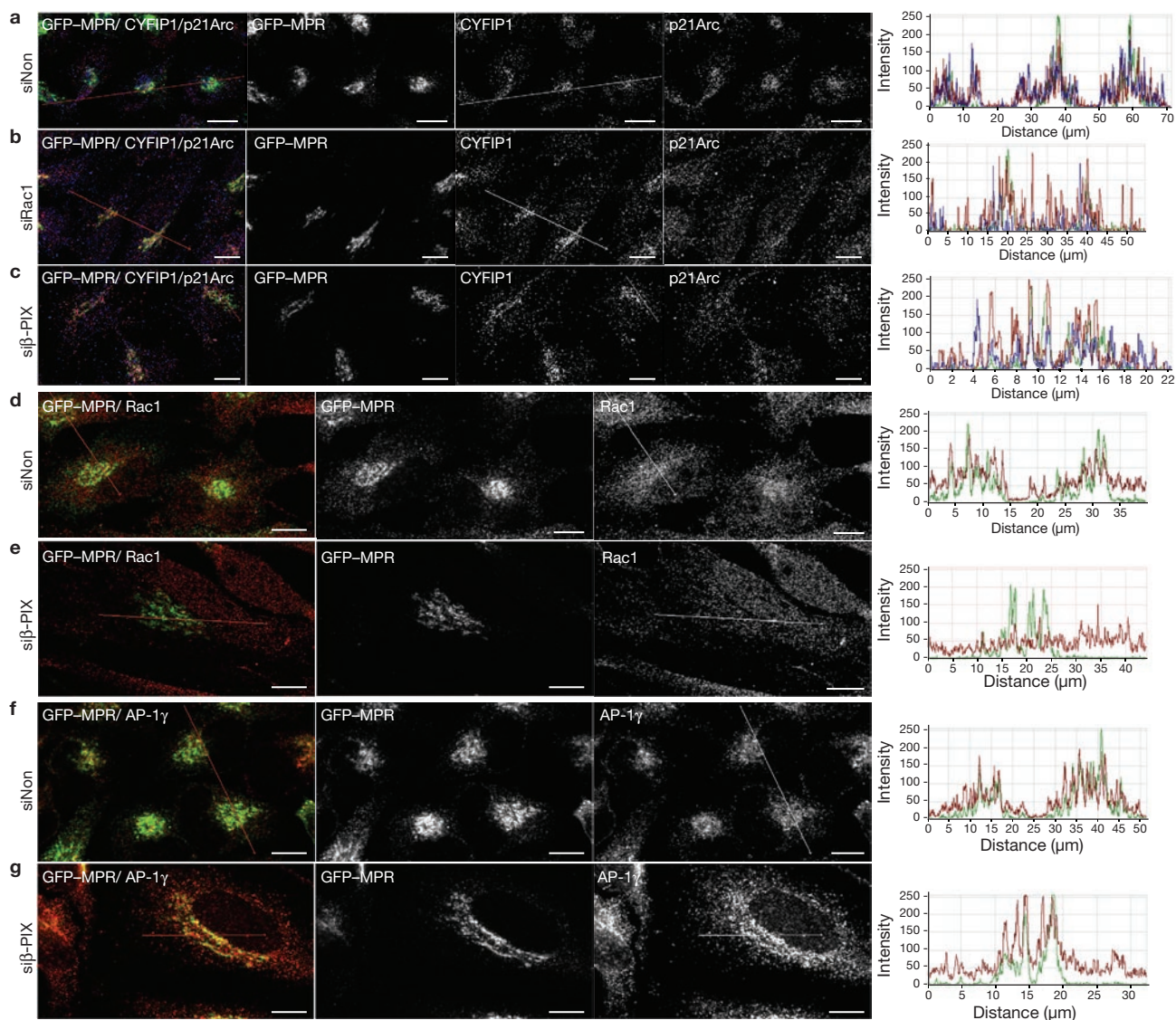


Figure 3 Rac1 and β -PIX control the recruitment of p21Arc but not CYFIP1 to the TGN. GFP-MPR-expressing HeLa cells incubated with the indicated siRNAs were labelled with anti-CYFIP1 (red) and anti-p21-Arc (blue) (a–c),

anti-Rac1 (red) or anti-AP-1 (red) (d, e) or anti-AP-1 γ (red) (f, g) and examined by confocal microscopy. A total of 20–25 cells from $n = 3$ independent experiments were analysed in each case. Scale bars, 10 μ m.

of HeLa cells²⁹ (Fig. 2a). A significant amount of p21Arc, a subunit of the Arp2/3 complex, was detected on these clathrin-coated and CYFIP-coated structures (Fig. 1b). In the absence of anti-CYFIP2 antibodies, a Myc-tagged CYFIP2 was expressed in HeLa cells. Myc-CYFIP2 was detected on enlarged, perinuclear, clathrin-AP-1-coated compartments (Fig. 1e, f) also containing CYFIP1 and Rab11 (Supplementary Information, Fig. S1b, c). They also contained a fraction of the endogenous cation-independent MPR (Supplementary Information, Fig. S1a) and the TfnR (Supplementary Information, Fig. S1d), although most of these receptors were detected in small vesicular structures surrounding the CYFIP2-positive compartments, suggesting that their trafficking is affected by overexpression of CYFIP2. However, these enlarged structures remained devoid of early EEA1 and late LAMP-1 endosomal markers (Supplementary Information, Fig. S1e, f). The GM-130-positive *cis*-Golgi remained unaffected (data not shown). Similar CYFIP2-positive and AP-1-positive enlarged structures were detected in CYFIP2-expressing cells by electron microscopy (Fig. 1g–k). Expression of

GFP-CYFIP1 also induced the formation of similar, enlarged structures (data not shown). Thus, endogenous CYFIP1 and ectopically expressed CYFIP2 associate with the TGN and to a smaller extent with recycling endosomes where clathrin-AP-1 coats are found³⁰.

CYFIP interacts with clathrin and Arf1 regulates its recruitment

The recruitments of clathrin-AP-1 coats and the CYFIP-containing complexes on synthetic membranes are coordinated, presumably by means of interactions between components of the two machineries⁸. To address this issue, we treated cells with brefeldin A (BFA), which prevents the Arf1 activation required for clathrin and AP-1 recruitment. Statistical image analysis indicated that this treatment also resulted in a loss of CYFIP1 from the TGN containing most of the GFP-MPR tail (Fig. 2a, b, d). This prompted us to perform co-immunoprecipitation experiments from cell lysates. Anti-CYFIP1 co-immunoprecipitated a significant fraction of clathrin heavy chain

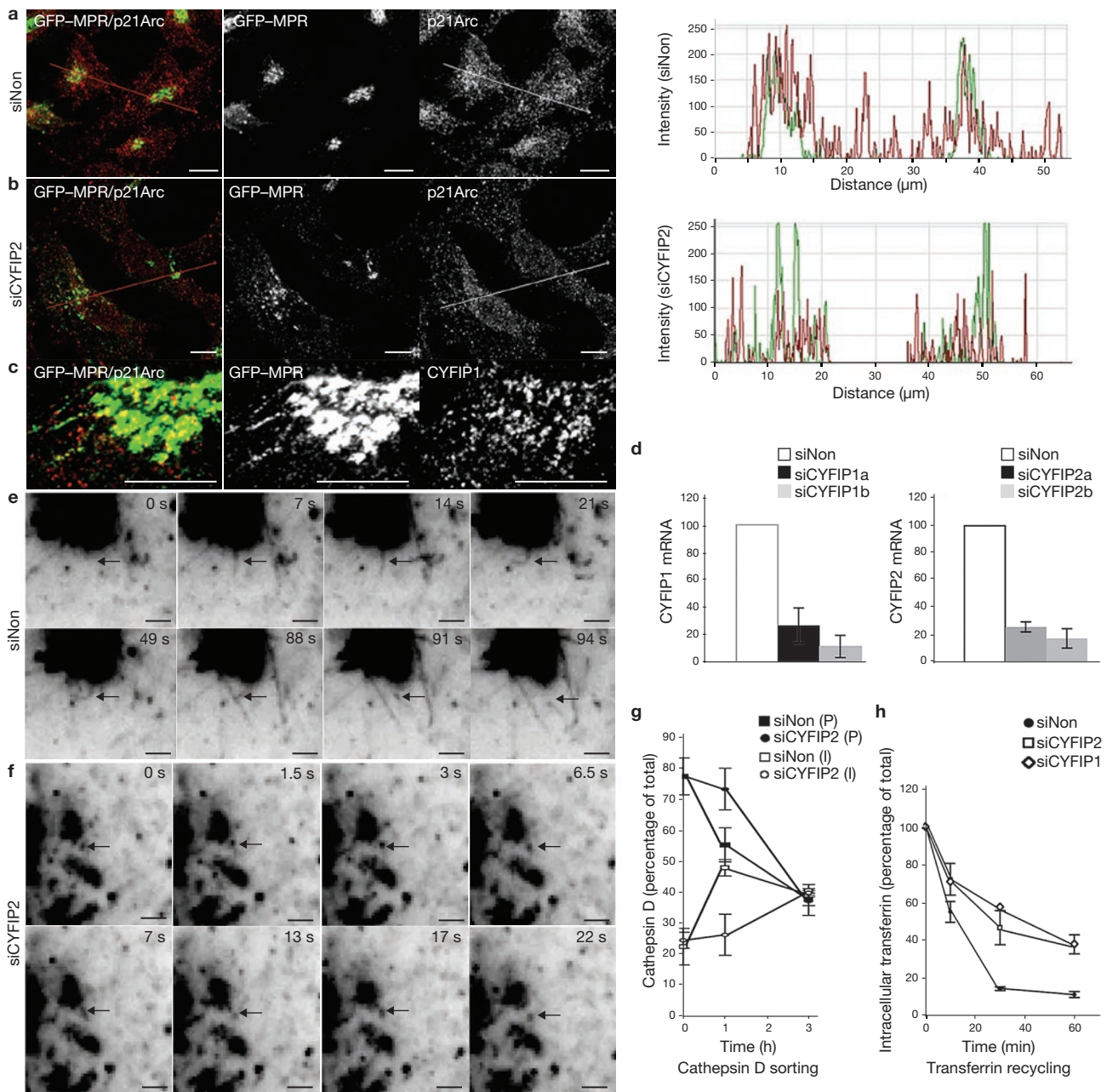


Figure 4 CYFIP2 depletion disrupts organelle integrity and decreases transport carrier biogenesis. GFP-MPR-expressing HeLa cells were treated with control siRNAs or with siRNAs targeting CYFIP2 or CYFIP1. **(a, b)** Cells were labelled with anti-p21Arc (red), and co-localization between GFP-MPR and p21Arc in the TGN region was analysed. A total of 20 cells from $n = 3$ independent experiments were analysed for each condition. **(c)** Confocal fluorescence analysis indicated that CYFIP1 localized along GFP-MPR tubules ($n = 20$ cells). Scale bars, 10 μm . **(d)** The levels of CYFIP1 and CYFIP2 mRNAs after the indicated knockdowns were measured by quantitative real-time (qRT) PCR; glyceraldehyde-3-phosphate dehydrogenase was used as a control ($n = 4$ independent experiments; data are shown as means \pm s.d.). **(e, f)** Cells were examined by time-lapse videomicroscopy. The number of GFP-MPR-positive

tubules exiting from the GFP-MPR-rich compartment was analysed as shown in Table 1. Scale bars, 2 μm . **(g)** HeLa cells were labelled with [^{35}S]methionine for 30 min, then pulse-chased for the indicated durations. Cathepsin D was immunoprecipitated from the lysates and analysed by SDS-PAGE. The relative levels of the precursor (P) and intermediate (I) forms were quantified relative to the total cathepsin D levels ($n = 3$ independent experiments; data are shown as means \pm s.d.). **(h)** To measure transferrin (Tfn) recycling, cells were starved for 1 h, then incubated with fluorescent-labelled Tfn for 1 h, and chased at 37 $^{\circ}\text{C}$ in the presence of unlabelled Tfn for the indicated durations. The amount of intracellular labelled Tfn was measured by fluorescence microscopy and quantified with ImageJ ($n = 3$ independent experiments for siNon and siCYFIP2; data are shown as means \pm s.d.).

(CHC), and anti-Myc co-immunoprecipitated a fraction of CYFIP1 from lysates of Myc-CYFIP2-expressing cells (Fig. 2f, g). The amino-terminal and carboxy-terminal domains of CYFIP2, both containing putative, evolutionarily conserved CHC-binding motifs also present

in CYFIP1 (Supplementary Information, Fig. S2), were found to interact with the N-terminal domain of CHC in a yeast two-hybrid system (Fig. 2h). The known interaction between CYFIP2 and NAP1 was used as a control. Consistent with these findings, siRNA (short interfering

Table 1 Biogenesis of GFP-MPR tail-containing tubular transport carriers in siRNA-treated HeLa cells

siRNA	No. of tubules growing from the TGN per cell per 2 min	Tubule length (μm)	No. of cells
siNon	4.3 \pm 1.02	5.9 \pm 2.8	40
siCYFIP2	1.72 \pm 0.99*	2 \pm 0.55*	50
siCYFIP1	1.53 \pm 0.99*		42
siN-WASP	2.07 \pm 0.77*	1.74 \pm 0.43*	25
siCdc42	3.05 \pm 1.14	3.44 \pm 1.61*	47
siRac1	1.98 \pm 0.81*	2.35 \pm 0.81*	100
si β -PIX	1.83 \pm 1.2*	1.59 \pm 0.42*	36

GFP-MPR-tail-expressing cells were incubated with the indicated siRNAs for 72 h. Exit of GFP-MPR tubules from the TGN region was monitored by time-lapse fluorescence microscopy. The interval between the acquisition of two consecutive images was 500 ms. $n = 5$ independent experiments were performed for siCYFIP2 and siCYFIP1, and $n = 3$ independent experiments for the other conditions; data are shown as means \pm s.d.; asterisk, $P < 0.0001$, ANOVA single-factor analysis, $\alpha = 0.05$.

RNA)-mediated CHC knockdown resulted in a loss of CYFIP1 from the GFP-MPR-tail-containing TGN as observed by fluorescence microscopy and statistical image analysis (Fig. 2c, d), and from membranes as detected by cell fractionation (Fig. 2e). Thus, clathrin-AP-1 coats and CYFIP-containing complexes were physically linked by means of CHC-CYFIP interactions, thereby explaining why Arf1 regulated their concomitant recruitment onto TGN membranes.

CYFIP activity requires N-WASP and Rac1

The CYFIP-containing complexes seem to be versatile, being able to associate with various downstream components to activate actin polymerization¹⁹. It was therefore crucial to determine which components regulate actin polymerization together with these modules at the TGN. We speculated that the formation of enlarged structures triggered by CYFIP2 expression resulted from higher actin polymerization around membranes. Indeed, these structures were enriched in p21Arc and surrounded by F-actin (Supplementary Information, Fig. S3a-c). We reasoned that knockdown of any component functioning together with CYFIP2 in actin polymerization would prevent the formation of these enlarged structures. Actin polymerization at the TGN may involve two GTPases previously shown to associate with clathrin-AP-1-coated membranes⁸: first, Cdc42, which activates Arp2/3 and is itself recruited in an Arf1-dependent manner by an as yet unknown mechanism^{31,32} and second, Rac1, which binds to CYFIP^{21,33}. Knockdown of Rac1, but not that of Cdc42, decreased the number of CYFIP2-enriched structures, as did latrunculin B, which prevents actin polymerization (Supplementary Information, Fig. S3e, f, h, j). Moreover, Rac1 was detected on these enlarged structures (Supplementary Information, Fig. S3d). Our proteomic studies using brain cytosol also detected WAVE1 and WAVE3, proteins predominantly expressed in brain¹⁹. In HeLa cells, their counterpart WAVE2 may activate Arp2/3. However, only knockdown of N-WASP or WASP, not that of WAVE2, decreased the number of CYFIP2-positive large structures (Supplementary Information, Fig. S3i, j). Taken together, these results indicate that CYFIP2 and Rac1 regulate actin nucleation at the TGN with N-WASP or WASP.

Rac1 and its exchange factor β -PIX regulate Arp2/3 recruitment to the TGN

Rac1, when activated by a specific exchange factor, could regulate the membrane association of CYFIP-containing complexes, their activity in Arp2/3-dependent actin polymerization, or both. We previously identified β -PIX as a unique Rho-GTPase exchange factor associated with clathrin-AP-1 coats⁸. Statistical image analyses indicated that knockdown of Rac1 (70% inhibition) decreased the amount of p21Arc, but not that of CYFIP1, on the GFP-MPR-tail-positive TGN (Fig. 3a;

Supplementary Information, Figs S3g and S4a, b). Moreover, knockdown of β -PIX (90% inhibition) resulted in a loss of Rac1 and p21Arc from the GFP-MPR-tail-rich perinuclear compartments without affecting the distributions of CYFIP1 and AP-1 (Fig. 3b, c; Supplementary Information, Fig. S4c, d). The siRNA-mediated knockdown of CYFIP1 or CYFIP2 (Fig. 4a, b, d; Supplementary Information, Fig. S4e-g) also resulted in a significant loss of p21Arc from the TGN. No changes were detected in the cell periphery. Knockdown of CYFIP2 did not result in a complete loss of CYFIP1 and did not drastically affect the stability of NAP1, another component of the CYFIP-containing protein complex (Supplementary Information, Fig. S4f, g), an observation which differs from others²⁷. Thus, Rac1 and β -PIX do not regulate the membrane association of CYFIP-containing complexes but rather their ability to recruit Arp2/3 complexes as nucleators of actin polymerization.

CYFIP1/2, Rac1, β -PIX and N-WASP promote clathrin-AP-1-coated carrier biogenesis *in vivo*

MPR trafficking depends on pleomorphic, clathrin-AP-1-coated tubular carriers that form at the TGN in an actin-dependent and microtubule-dependent manner²⁹. Endogenous CYFIP1 was detected at proximal sites and along most of the GFP-MPR-tail-labelled tubules (77.6 \pm 7.8% s.d.; $n = 20$ cells) still connected with the TGN (Fig. 4c). We therefore analysed the formation of these tubules in cells depleted of different regulators of actin polymerization. Consistent with our previous studies²⁹, an average of 4.3 \pm 1.0 GFP-MPR-tail-labelled tubules with an average length of 5.9 \pm 2.8 μm were formed within 2 min in control cells (Fig. 4e and Table 1; Supplementary Information, Movie 1). Both the number and the length of these tubules were significantly decreased in cells depleted of CYFIP1, CYFIP2, N-WASP, Rac1 or β -PIX by siRNA treatment (Fig. 4f and Table 1; Supplementary Information, Movies 2 and 4-9). In contrast, knockdown of Cdc42 had a milder effect on the dynamics of tubules that contained GFP-MPR tails (Table 1), although it affected the integrity of the TGN containing GFP-MPR tails (Supplementary Movie 8) or endogenous MPR, as did knockdowns of CYFIP1 or CYFIP2, N-WASP, Rac1 (Supplementary Information, Figs S5 and S6a) or Abi1 (not shown). CYFIP1 or CYFIP2 knockdowns also resulted in redistribution of the GFP-MPR tail to TfnR-rich compartments, presumably recycling endosomes (Supplementary Information, Figs S4h and S6b). However, the GM-130-positive *cis*-Golgi (Supplementary Information, Fig. S6d), and also the integrity of microtubules (not shown), remained unaffected. In contrast, knockdown of WAVE2 resulted in compaction of the TGN (Supplementary Information, Fig. S5), suggesting that a balance between the activity of N-WASP and WAVE2 might regulate compartment integrity. We conclude that CYFIP1 and CYFIP2, Rac1,

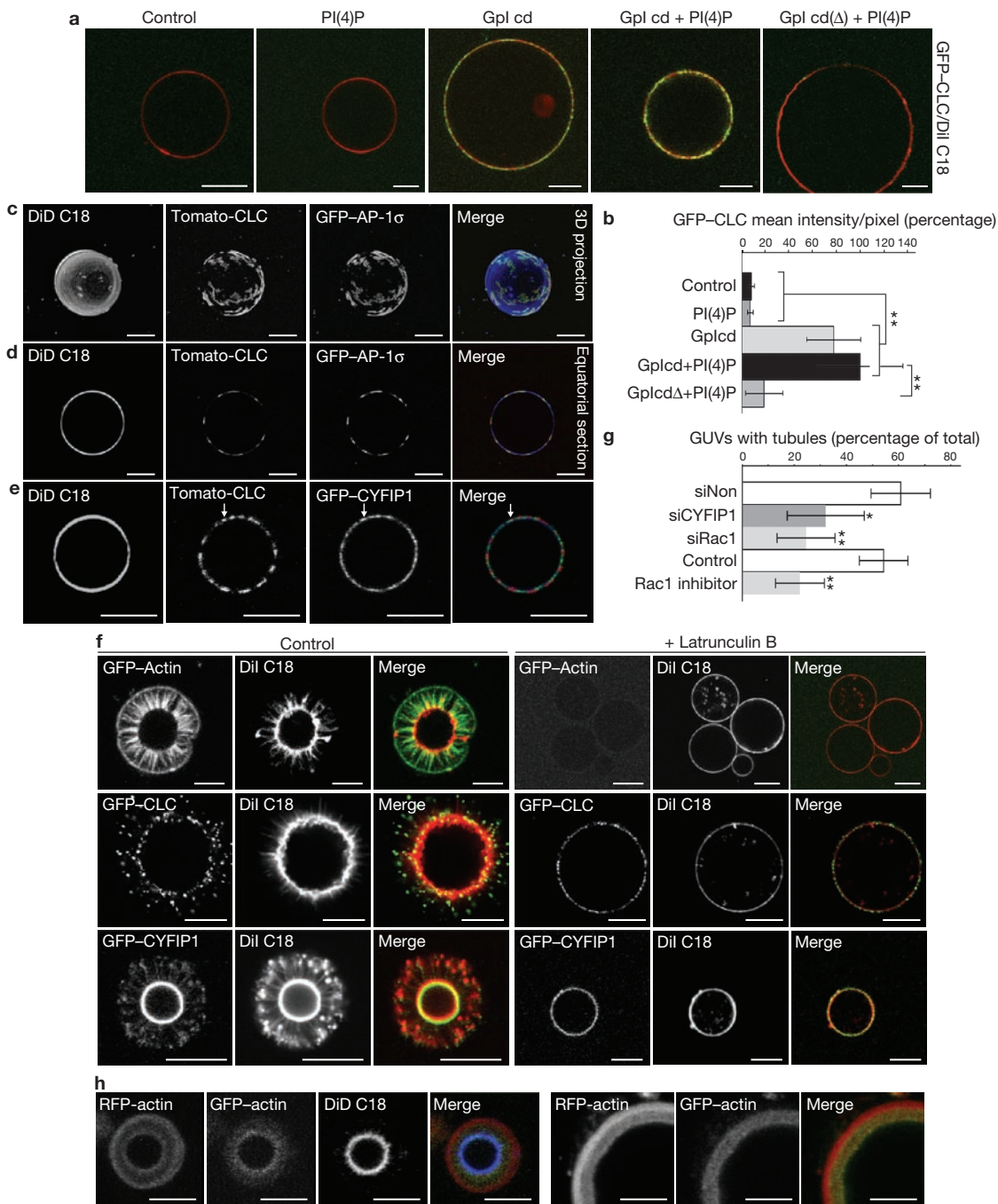


Figure 5 Reconstitution of clathrin-AP-1-coated carrier biogenesis on model membranes. **(a, b)** DiI C18-labelled giant unilamellar vesicles (GUVs), alone, or containing only PI(4)P, only varicella zoster virus glycoprotein I (Gpl) cytoplasmic domains (cd), or both Gpl tails and PI(4)P, or PI(4)P and the Gpl cytoplasmic domain devoid of sorting signals (GplcdΔ), were incubated in the presence of GTP-γS with porcine brain cytosol spiked with cytosol of CLC-EGFP-expressing cells. They were then imaged by confocal microscopy **(a)**, and CLC-EGFP intensities **(b)** were determined ($n = 3$ independent experiments; data are shown as means \pm s.d.; $P_{PI(4)P/no PI(4)P} = 0.386$, at least 7 GUVs per condition; $P_{Gpl/no Gpl (no PI(4)P)} = 9.88 \times 10^{-9}$, 10 GUVs per condition; $P_{Gpl/ no Gpl (with PI(4)P)} = 2.18 \times 10^{-7}$, 7 GUVs per condition; $P_{Gpl + PI(4)P/Gpl (no PI(4)P)} = 0.088$, at least 7 GUVs per condition; $P_{Gpl/Gplcd (with PI(4)P)} = 2.5 \times 10^{-23}$, at least 43 GUVs per condition; analysis of variance (ANOVA) single-factor analysis). **(c–e)** DiI C18-labelled GUVs with Gpl cytoplasmic domains and PI(4)P were incubated in the presence of GTP-γS and porcine brain cytosol spiked with a mixture of cytosols from cells expressing dTomato-CLC and EGFP-AP-1σ or GFP-CYFIP1. The samples were imaged by confocal microscopy. **(f)** GUVs

with Gpl tails and PI(4)P were incubated, as in **(c)**, with an ATP-regenerating system, in the absence (left panels) or the presence (right panels) of 50 μM latrunculin B (25 min). **(g)** DiI C18-labelled GUVs with Gpl tails and PI(4)P were incubated with cytosols of EGFP-actin-expressing HEK cells treated with the indicated siRNAs or with 100 nM Rac1 inhibitor (NSC23766). Actin polymerization and tubule formation were analysed by confocal microscopy, and the number of GUVs displaying EGFP-actin tubes is shown as a percentage of the total DiI C18-positive GUVs ($n = 3$ independent experiments for siRNA-treated cells and $n = 5$ independent experiments for Rac1 inhibitor; data are shown as means \pm s.d.; more than 250 GUVs were analysed for each condition; $P_{siCYFIP1} = 0.02$, $P_{siRac1} = 0.0017$ compared with control siNon; $P_{Rac1 inhibitor} = 0.002$ compared with control cells; ANOVA single-factor analysis). **(h)** DiI C18-labelled GUVs with Gpl cytoplasmic domains and PI(4)P were incubated at 37 °C in the presence of GTP-γS and porcine brain cytosol spiked with cytosol from RFP-actin-expressing HEK cells. After 15 min, cytosol from EGFP-actin-expressing cells was added, and the GUVs were incubated for a further 10 min and analysed by confocal microscopy. Scale bars, 10 μm.

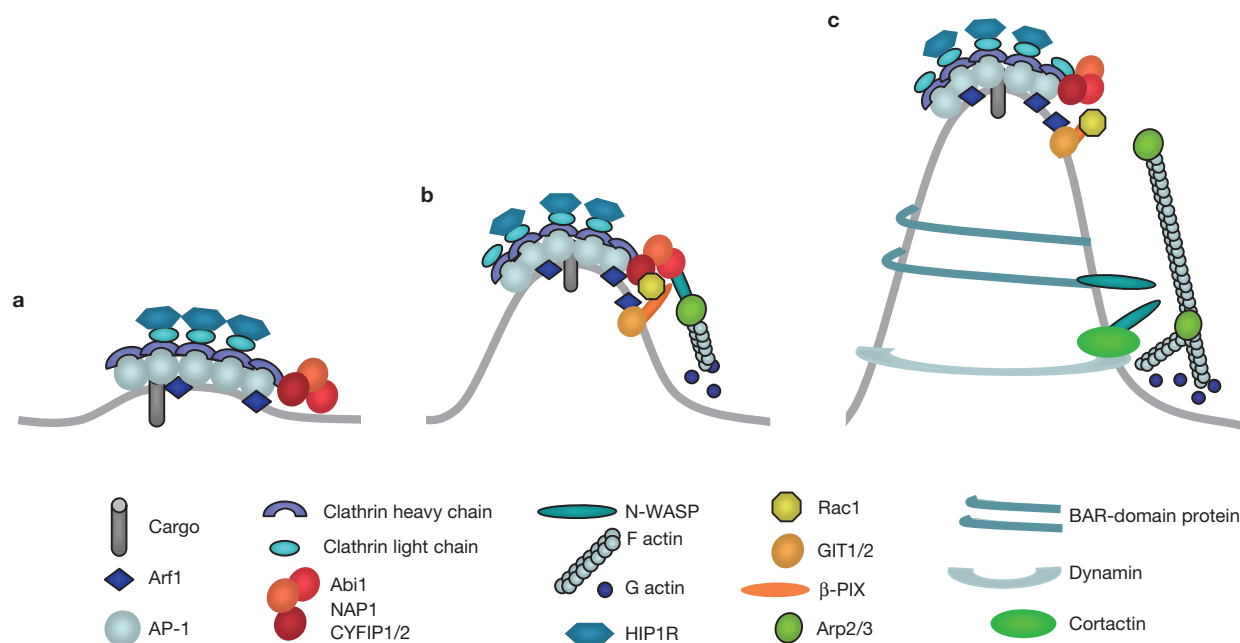


Figure 6 Model of clathrin-AP-1-coated carrier biogenesis. (a) Recruitment of Arf1-dependent coat and actin nucleation complex. Arf1 activation triggers the recruitment of AP-1 and clathrin to TGN membranes, leading to cargo sorting. The CYFIP-Abi-NAP1 complex is recruited at the edges of the clathrin-AP-1-coated subdomains of the TGN. HIP1R binding to clathrin light chains could prevent actin polymerization on the surface of clathrin coats. (b) Rac1-dependent tubule formation (early stages). Rac1, activated by its GEF β -PIX,

β -PIX and N-WASP are essential for maintaining the integrity of the TGN and for promoting the formation of GFP-MPR-containing tubular carriers from this organelle.

CYFIP regulates cargo transport

To address the functional importance of the CYFIP-containing module in biosynthetic transport, we performed classical pulse-chase experiments to monitor the MPR-dependent transport of the newly synthesized cathepsin D to lysosomes. This lysosomal enzyme is synthesized as a precursor of relative molecular mass (M_r) 55,000 (55K) that is then processed to a M_r 45K intermediate form on delivery to acidified endosomal compartments. This processing was significantly decreased after CYFIP2 knockdown (Fig. 4g; Supplementary Information, Fig. S7a), to an extent similar to that observed after knockdown of the clathrin light chain³⁴.

We also monitored the recycling of the cell-surface GFP-MPR tail back to the TGN in GFP-MPR-tail-expressing HeLa cells. Whereas in control cells the internalized anti-GFP antibodies rapidly localized to the perinuclear region together with the bulk of GFP-MPR tails, in CYFIP2-depleted cells they remained in peripheral structures (Supplementary Information, Fig. S7b, c). This would be consistent with the observation that in CYFIP1-depleted or CYFIP2-depleted cells GFP-MPR tails are more abundant in TfrR-positive endocytic compartments (Supplementary Information, Fig. S6f). CYFIP1 or CYFIP2 knockdown also decreased the recycling rate of endocytosed transferrin, which accumulated in peripheral structures (Fig. 4h; Supplementary Information, Fig. S7d). However, endocytosis of transferrin remained unaffected (Supplementary Information, Fig. S7e).

which forms a complex with the Arf1-GAP GIT1 and/or GIT2, binds to CYFIP and activates the actin nucleation complex, leading to N-WASP-dependent activation of Arp2/3 and actin polymerization towards the TGN membrane during the initial stages of tubular carrier formation. (c) Tubulin elongation (late stages). BAR-domain proteins, dynamin2 and cortactin bind to tubular membranes. These molecules can bind N-WASP and thus sustain Arp2/3-dependent actin polymerization during tubule elongation and fission.

Although it is possible that CYFIP1 and CYFIP2 are involved in transport from these peripheral structures, these results may also be due to indirect effects (such as TGN fragmentation).

Clathrin-AP-1-coated carrier biogenesis on model membranes

Clathrin-AP-1 coats and CYFIP-containing actin nucleation modules bind on model membranes minimally composed of sorting signals present in the cytoplasmic domains of specific cargoes, namely Arf1 and PI(4)P (ref. 8). To image these model membranes and their bound components, we incubated functionalized giant unilamellar vesicles (GUVs) with pig brain cytosol spiked with cytosol of cells stably expressing various fluorescent-tagged proteins in the presence of the non-dissociating GTP analogue GTP- γ S, and then imaged these GUVs by fluorescence microscopy. Consistent with our previous studies, efficient clathrin binding depended on the presence of intact sorting motifs in cargo cytoplasmic tails (Fig. 5a, b). When ATP was absent, clathrin and AP-1 co-assembled on these GUVs (Fig. 5c, d), where CYFIP1 was also present (Fig. 5e). In the presence of ATP, tubular membrane extensions labelled with the lipophilic dye DiI (1,1'-dioctadecyl-3,3,3',3'-tetramethylindocarbocyanine perchlorate) were detected (Fig. 5f; Supplementary Information, Fig. S8a and Movie 3). Clathrin was present at the tips of these tubules, as in HeLa cells²⁹. CYFIP1 was also detected at the tips and along the tubules (Fig. 5f), as observed in HeLa cells (Fig. 4d). In the presence of latrunculin B, as in the absence of ATP, these tubular membrane extensions were not formed; clathrin and CYFIP1 remained on GUV surfaces. Similarly, knockdown of CYFIP1 (50–60% inhibition) or Rac1 (70% inhibition) in GFP-actin-expressing cells decreased tubule formation by more than 50%, as did NSC23766, a

Rac1 inhibitor (Fig. 5g; Supplementary Information, Fig. S8b). A dense F-actin meshwork surrounded the tubules forming from GUVs (Fig. 5f). In pulse-chase experiments in which red fluorescent protein (RFP)-labelled actin was added first, followed by GFP-actin, GFP-actin was detectable near the membrane, thus indicating that actin polymerized towards the GUV membranes (Fig. 5h). We conclude that ATP-driven actin polymerization was sufficient to generate tubules from GUVs provided that clathrin coats and CYFIP-containing complexes were present on membranes and that Rac1 activated actin polymerization.

DISCUSSION

Our study reveals that the biogenesis of clathrin-AP-1-coated transport carriers results from the coordinated activities of coat components and actin nucleation machineries. It elucidates the functional links between Arf1, clathrin-AP-1 coats, CYFIP-containing complexes, Rac1, its exchange factor β -PIX, and N-WASP, which together regulate Arp2/3-dependent actin polymerization, membrane remodelling and transport carrier biogenesis. Thus, our study provides a protein-network-based mechanism that not only links different machineries at the TGN but also allows for the sequential coordination of Arf1 and Rac1 signalling. This mechanism provides complementary but independent levels of regulation during the early stages of post-Golgi transport.

Actin dynamics is involved in several aspects of post-Golgi transport; however, the associated protein networks are poorly characterized. So far, HIP1R, which binds to clathrin light chains, has been shown to inhibit actin polymerization during post-Golgi transport of MPRs^{13,34} and endocytosis. Our study demonstrates the functional importance of an entire protein network in which the interaction between CHC and CYFIP is central to the coordination of coat assembly, actin polymerization and membrane remodelling during clathrin-AP-1-coated carrier biogenesis. It remains possible that additional interactions exist between AP-1 subunits and other subunits of the CYFIP-containing complexes (Abi, NAP1 and HSPC 300). It is likely that these complexes bind to the edges of clathrin-AP-1 coats, where CHC N-terminal domains protruding towards the membrane would be available for interactions with CYFIP. In contrast, HIP1R interacts with clathrin light chains located on the surface of clathrin coats. Therefore HIP1R covering the surface of clathrin coats may impair the accessibility of CYFIP-containing complexes inside these coats, thus preventing actin polymerization at this location.

Actin dynamics at the Golgi complex is regulated by Rho GTPases, whose activity is controlled by the Arf1 GTPase. However, the mechanisms connecting Arf1 and Rho signalling have so far remained elusive. Membrane-bound Arf1•GTP recruits ARHGAP10, a Cdc42 GTPase-activating protein (GAP), and therefore downregulates Arp2/3 activity and F-actin dynamics through the control of Golgi-associated Cdc42, thereby regulating Golgi integrity³¹. Rac1 is also recruited to the Golgi in an Arf1-dependent manner^{35,36}. Its overexpression leads to the formation of enlarged intracellular compartments surrounded by actin³⁷, as observed here after CYFIP overexpression. Our study highlights a multi-step process in which Arf1 controls the recruitment of both clathrin-AP1 coats and CYFIP-containing complexes, a process requiring interactions between CHC and CYFIP. Rac1 is clearly dispensable for CYFIP recruitment to the TGN. On clathrin-AP-1-coated model membranes we have also identified the Arf1-GAPs GIT1 or GIT2 and the Rho guanine nucleotide exchange factor (GEF) β -PIX⁸, which is known to form a complex³⁸. This study illustrates a role for β -PIX in

Rac1-dependent actin polymerization on TGN membranes. In a similar manner to Rac1, it does not contribute to the recruitment of either clathrin-AP-1 coats or CYFIP-containing complexes. However, after a β -PIX-mediated nucleotide exchange, activated Rac1 could in a later step bind to CYFIP^{21,33}, thereby leading to N-WASP-dependent, WASP-dependent and Arp2/3-dependent actin polymerization, membrane remodelling and formation of clathrin-AP-1-coated carriers. Thus, the control of Arf1-dependent Rac1 signalling at the TGN seems to be more complex than previously expected, implicating different but interconnected levels of regulation based on different types of protein-protein interaction (Fig. 6). Several other studies have illustrated the role of Rho GTPases in post-Golgi transport. Cdc42 regulates membrane traffic to the basolateral membrane of polarized cells^{39,40}. The Golgi-associated Cdc42 exchange factor FGD1 (faciogenital dysplasia protein 1) regulates the post-Golgi transport of various cargoes to the osteoblast surface and the formation of VSV-G (vesicular stomatitis virus G)-containing tubules at the TGN⁴¹. It therefore seems that Rac1 and Cdc42 regulate actin dynamics and protein transport along different routes of post-Golgi traffic.

Actin polymerization is thought to occur during the late stages of transport carrier biogenesis. This notion arises from the molecules that connect membranes and the actin cytoskeleton identified so far. Thus, the large GTPase dynamin2, which mediates carrier fission, binds the actin-interacting protein cortactin during post-Golgi transport¹⁴ or endocytosis⁴². Several BAR (Bin-Amphiphysin-Rvs)-domain-containing proteins, which sense the curvature of tubular membranes, bind not only dynamin but also N-WASP⁴³. Indeed, these proteins are detected by quantitative proteomics when tubular extensions are allowed to form from clathrin-AP-1-coated synthetic membranes (C. Stange, C. Czupalla and B. Hoflack, unpublished observation). Our study strongly suggests that actin polymerization also occurs during the early stages of clathrin-AP-1-coated carrier biogenesis when TGN membranes have been primed with clathrin coats and their bound CYFIP-containing complexes. Actin polymerization, as shown here, occurs towards membranes and could thus provide the forces necessary to deform membranes so as to generate tubular transport carriers. It is likely that lipid modifications and/or partition also accompany membrane remodelling. BAR-domain-containing proteins that bind to tubular membrane extensions could then stabilize this process and, together with N-WASP, further sustain actin polymerization. These molecular mechanisms could be similar to those regulating endocytosis, in which the recruitment of clathrin to the plasma membrane precedes the recruitment of N-WASP, Arp2/3 and actin, and actin polymerization towards membranes provides the forces needed for endocytic vesicle formation^{16,44–46}.

Whereas our study illustrates the functional importance of coordinating protein sorting, coat assembly, actin and membrane remodelling during post-Golgi transport, previous studies in *Drosophila melanogaster* have implicated CYFIP (Sra1, PIR) proteins in neuronal development⁴⁷. Several proteins shown to connect Arf1-dependent clathrin-AP-1 coat assembly and Rac1-dependent actin polymerization (ref. 8 and this study) are associated with human learning disability. Mutations in genes encoding AP-1 σ 2 (refs 48, 49) and p21 activated kinase 3 (PAK3)⁵⁰, a kinase that regulates β -PIX activity, cause the X-linked mental retardation syndrome. CYFIP1 and CYFIP2 link this pathway to the fragile-X mental retardation protein (FMRP) that is absent in the most common form of monogenic mental retardation^{21,51}. This strongly indicates that

sorting and actin polymerization may be perturbed in these cognitive disorders. In *Caenorhabditis elegans*, the AP-1 μ 1 subunit has a function in polarized receptor trafficking to dendrites^{52,53}, suggesting that dysfunctions of clathrin-dependent and AP-1-dependent sorting supported by actin polymerization may impair the normal trafficking of some neuronal receptors or cell adhesion molecules. In the absence of a functional FMRP, a CYFIP interactor, the trafficking of AMPA (α -amino-3-hydroxy-5-methyl-4-isoxazole propionic acid) receptors (especially glutamate receptors 1 and 5) to dendrites is impaired^{54,55}. Synaptic AMPA receptors are stored in recycling endosomes, from where they can be recruited to the surface of synapses on stimulation⁵⁶. Accordingly, AP-1 μ and Rab11 regulate glutamate receptor 1 trafficking^{57,58}. Thus, it is an exciting challenge to identify the specific cargoes whose trafficking is altered in the absence of components that regulate clathrin-dependent and AP-1-dependent protein transport and actin nucleation, to gain a better understanding of the molecular bases of these neurological disorders. □

METHODS

Methods and any associated references are available in the online version of the paper at <http://www.nature.com/naturecellbiology/>

Note: Supplementary Information is available on the Nature Cell Biology website.

ACKNOWLEDGEMENTS

We thank the members of the different laboratories for their helpful discussions and critical comments. D. Thiel provided technical assistance. We thank M. Zerial, T. Wassmer and C. Antos for their critical reading of the manuscript. This work was supported in part by grants from the Deutsche Forschungsgemeinschaft (TRR 13/1-2010, HO 2584/1-1, HO 2584/2-1, HO 2584/6-1, HO 2584/8-1, HO 2584/9-1), the German Ministry of Research (BMBF) (0313815B) and Dresden University of Technology (HWP-1207). T.Kirchhausen's research was supported by the NIH grant GM075252.

AUTHOR CONTRIBUTIONS

M.A. designed, performed and analysed the *in vivo* experiments. C.S. designed, performed and analysed the *in vitro* recruitment experiments. I.P. performed the quantitative real-time PCR experiments and yeast two-hybrid analyses. G.R. performed the electron microscopy. T.B., A.S. and T.K. provided key reagents. B.H. designed and analysed experiments, and wrote the manuscript with M.A. and C.S.

COMPETING FINANCIAL INTERESTS

The authors declare no competing financial interests.

Published online at <http://www.nature.com/naturecellbiology>

Reprints and permissions information is available online at <http://npg.nature.com/reprintsandpermissions/>

- Ghosh, P., Dahms, N. M. & Kornfeld, S. Mannose 6-phosphate receptors: new twists in the tale. *Nature Rev. Mol. Cell Biol.* **4**, 202–212 (2003).
- Edeling, M. A., Smith, C. & Owen, D. Life of a clathrin coat: insights from clathrin and AP structures. *Nature Rev. Mol. Cell Biol.* **7**, 32–44 (2006).
- Bonifacino, J. S. & Glick, B. S. The mechanisms of vesicle budding and fusion. *Cell* **116**, 153–166 (2004).
- Godi, A. *et al.* ARF mediates recruitment of PtdIns-4-OH kinase-beta and stimulates synthesis of PtdIns(4,5)P₂ on the Golgi complex. *Nature Cell Biol.* **1**, 280–287 (1999).
- D'Souza-Schorey, C. & Chavrier, P. ARF proteins: roles in membrane traffic and beyond. *Nature Rev. Mol. Cell Biol.* **7**, 347–358 (2006).
- Lee, I., Doray, B., Govero, J. & Kornfeld, S. Binding of cargo sorting signals to AP-1 enhances its association with ADP ribosylation factor 1-GTP. *J. Cell Biol.* **180**, 467–472 (2008).
- Le Borgne, R. & Hoflack, B. Mannose 6-phosphate receptors regulate the formation of clathrin-coated vesicles in the TGN. *J. Cell Biol.* **137**, 335–345 (1997).
- Baust, T., Czupalla, C., Krause, E., Bourel-Bonnet, L. & Hoflack, B. Proteomic analysis of adaptor protein 1A coats selectively assembled on liposomes. *Proc. Natl Acad. Sci. USA* **103**, 3159–3164 (2006).
- Pelish, H. E. *et al.* Secramine inhibits Cdc42-dependent functions in cells and Cdc42 activation *in vitro*. *Nature Chem. Biol.* **2**, 39–46 (2006).
- Salvarezza, S. B. *et al.* LIM kinase 1 and cofilin regulate actin filament population required for dynamin-dependent apical carrier fission from the trans-Golgi network. *Mol. Biol. Cell* **20**, 438–451 (2009).
- Egea, G., Lazaro-Dieguez, F. & Vilella, M. Actin dynamics at the Golgi complex in mammalian cells. *Curr. Opin. Cell Biol.* **18**, 168–178 (2006).
- Kondylis, V., van Nispen tot Pannerden, H. E., Herpers, B., Friggi-Grelin, F. & Rabouille, C. The golgi comprises a paired stack that is separated at G2 by modulation of the actin cytoskeleton through Abi and Scar/WAVE. *Dev. Cell* **12**, 901–915 (2007).
- Carreno, S., Engqvist-Goldstein, A. E., Zhang, C. X., McDonald, K. L. & Drubin, D. G. Actin dynamics coupled to clathrin-coated vesicle formation at the trans-Golgi network. *J. Cell Biol.* **165**, 781–788 (2004).
- Cao, H. *et al.* Actin and Arf1-dependent recruitment of a cortactin-dynamin complex to the Golgi regulates post-Golgi transport. *Nature Cell Biol.* **7**, 483–492 (2005).
- Engqvist-Goldstein, A. E. *et al.* RNAi-mediated Hip1R silencing results in stable association between the endocytic machinery and the actin assembly machinery. *Mol. Biol. Cell* **15**, 1666–1679 (2004).
- Kaksonen, M., Toret, C. P. & Drubin, D. G. Harnessing actin dynamics for clathrin-mediated endocytosis. *Nature Rev. Mol. Cell Biol.* **7**, 404–414 (2006).
- McNiven, M. A. & Thompson, H. M. Vesicle formation at the plasma membrane and trans-Golgi network: the same but different. *Science* **313**, 1591–1594 (2006).
- Welch, M. D., Iwamatsu, A. & Mitchison, T. J. Actin polymerization is induced by Arp2/3 protein complex at the surface of *Listeria monocytogenes*. *Nature* **385**, 265–269 (1997).
- Takenawa, T. & Suetsugu, S. The WASP-WAVE protein network: connecting the membrane to the cytoskeleton. *Nature Rev. Mol. Cell Biol.* **8**, 37–48 (2007).
- Campellone, K. G., Webb, N. J., Znameroski, E. A. & Welch, M. D. WHAMM is an Arp2/3 complex activator that binds microtubules and functions in ER to Golgi transport. *Cell* **134**, 148–161 (2008).
- Schenck, A. *et al.* CYFIP/Sra-1 controls neuronal connectivity in *Drosophila* and links the Rac1 GTPase pathway to the fragile X protein. *Neuron* **38**, 887–898 (2003).
- Eden, S., Rohatgi, R., Podtelejnikov, A. V., Mann, M. & Kirschner, M. W. Mechanism of regulation of WAVE1-induced actin nucleation by Rac1 and Nck. *Nature* **418**, 790–793 (2002).
- Kunda, P., Craig, G., Dominguez, V. & Baum, B. Abi, Sra1, and Kette control the stability and localization of SCAR/WAVE to regulate the formation of actin-based protrusions. *Curr. Biol.* **13**, 1867–1875 (2003).
- Steffen, A. *et al.* Sra-1 and Nap1 link Rac to actin assembly driving lamellipodia formation. *EMBO J.* **23**, 749–759 (2004).
- Gautreau, A. *et al.* Purification and architecture of the ubiquitous Wave complex. *Proc. Natl Acad. Sci. USA* **101**, 4379–4383 (2004).
- Bogdan, S., Stephan, R., Lobke, C., Mertens, A. & Klambt, C. Abi activates WASP to promote sensory organ development. *Nature Cell Biol.* **7**, 977–984 (2005).
- Innocenti, M. *et al.* Abi1 regulates the activity of N-WASP and WAVE in distinct actin-based processes. *Nature Cell Biol.* **7**, 969–976 (2005).
- Schenck, A., Bardoni, B., Moro, A., Bagni, C. & Mandel, J. L. A highly conserved protein family interacting with the fragile X mental retardation protein (FMRP) and displaying selective interactions with FMRP-related proteins FXR1P and FXR2P. *Proc. Natl Acad. Sci. USA* **98**, 8844–8849 (2001).
- Waguri, S. *et al.* Visualization of TGN to endosome trafficking through fluorescently labeled MPR and AP-1 in living cells. *Mol. Biol. Cell* **14**, 142–155 (2003).
- Folsch, H., Pypaert, M., Maday, S., Pelletier, L. & Mellman, I. The AP-1A and AP-1B clathrin adaptor complexes define biochemically and functionally distinct membrane domains. *J. Cell Biol.* **163**, 351–362 (2003).
- Dubois, T. *et al.* Golgi-localized GAP for Cdc42 functions downstream of ARF1 to control Arp2/3 complex and F-actin dynamics. *Nature Cell Biol.* **7**, 353–364 (2005).
- Fucini, R. V., Chen, J. L., Sharma, C., Kessels, M. M. & Stammes, M. Golgi vesicle proteins are linked to the assembly of an actin complex defined by mAbp1. *Mol. Biol. Cell* **13**, 621–631 (2002).
- Kobayashi, K. *et al.* p140Sra-1 (specifically Rac1-associated protein) is a novel specific target for Rac1 small GTPase. *J. Biol. Chem.* **273**, 291–295 (1998).
- Poupon, V. *et al.* Clathrin light chains function in mannose phosphate receptor trafficking via regulation of actin assembly. *Proc. Natl Acad. Sci. USA* **105**, 168–173 (2008).
- Kraynov, V. S. *et al.* Localized Rac activation dynamics visualized in living cells. *Science* **290**, 333–337 (2000).
- Faucherre, A. *et al.* Lowe syndrome protein OCRL1 interacts with Rac GTPase in the trans-Golgi network. *Hum. Mol. Genet.* **12**, 2449–2456 (2003).
- Jou, T. S. *et al.* Selective alterations in biosynthetic and endocytic protein traffic in Madin-Darby canine kidney epithelial cells expressing mutants of the small GTPase Rac1. *Mol. Biol. Cell* **11**, 287–304 (2000).
- Premont, R. T. *et al.* The GIT/PIX complex: an oligomeric assembly of GIT family ARF GTPase-activating proteins and PIX family Rac1/Cdc42 guanine nucleotide exchange factors. *Cell Signal.* **16**, 1001–1011 (2004).
- Kroschewski, R., Hall, A. & Mellman, I. Cdc42 controls secretory and endocytic transport to the basolateral plasma membrane of MDCK cells. *Nature Cell Biol.* **1**, 8–13 (1999).
- Musch, A., Cohen, D., Kreitzer, G. & Rodriguez-Boulant, E. cdc42 regulates the exit of apical and basolateral proteins from the trans-Golgi network. *EMBO J.* **20**, 2171–2179 (2001).
- Egorov, M. V. *et al.* Faciogenital dysplasia protein (FGD1) regulates export of cargo proteins from the golgi complex via Cdc42 activation. *Mol. Biol. Cell* **20**, 2413–2427 (2009).
- McNiven, M. A. *et al.* Regulated interactions between dynamin and the actin-binding protein cortactin modulate cell shape. *J. Cell Biol.* **151**, 187–198 (2000).
- Dawson, J. C., Legg, J. A. & Machesky, L. M. Bar domain proteins: a role in tubulation, scission and actin assembly in clathrin-mediated endocytosis. *Trends Cell Biol* **16**, 493–498 (2006).

44. Merrifield, C. J., Feldman, M. E., Wan, L. & Almers, W. Imaging actin and dynamin recruitment during invagination of single clathrin-coated pits. *Nature Cell Biol.* **4**, 691–698 (2002).
45. Merrifield, C. J., Qualmann, B., Kessels, M. M. & Almers, W. Neural Wiskott Aldrich syndrome protein (N-WASP) and the Arp2/3 complex are recruited to sites of clathrin-mediated endocytosis in cultured fibroblasts. *Eur. J. Cell Biol.* **83**, 13–18 (2004).
46. Merrifield, C. J., Perrais, D. & Zenisek, D. Coupling between clathrin-coated-pit invagination, cortactin recruitment, and membrane scission observed in live cells. *Cell* **121**, 593–606 (2005).
47. Schenck, A. *et al.* WAVE/SCAR, a multifunctional complex coordinating different aspects of neuronal connectivity. *Dev. Biol.* **274**, 260–270 (2004).
48. Borck, G. *et al.* Clinical, cellular, and neuropathological consequences of *AP1S2* mutations: further delineation of a recognizable X-linked mental retardation syndrome. *Hum. Mutat.* **29**, 966–974 (2008).
49. Tarpey, P. S. *et al.* Mutations in the gene encoding the Sigma 2 subunit of the adaptor protein 1 complex, *AP1S2*, cause X-linked mental retardation. *Am. J. Hum. Genet.* **79**, 1119–1124 (2006).
50. Allen, K. M. *et al.* *PAK3* mutation in nonsyndromic X-linked mental retardation. *Nature Genet.* **20**, 25–30 (1998).
51. Nowicki, S. T. *et al.* The Prader–Willi phenotype of fragile X syndrome. *J. Dev. Behav. Pediatr.* **28**, 133–138 (2007).
52. Dwyer, N. D., Adler, C. E., Crump, J. G., L'Etoile, N. D. & Bargmann, C. I. Polarized dendritic transport and the AP-1 mu1 clathrin adaptor UNC-101 localize odorant receptors to olfactory cilia. *Neuron* **31**, 277–287 (2001).
53. Sakaguchi-Nakashima, A., Meir, J. Y., Jin, Y., Matsumoto, K. & Hisamoto, N. LRK-1, a *C. elegans* PARK8-related kinase, regulates axonal-dendritic polarity of SV proteins. *Curr. Biol.* **17**, 592–598 (2007).
54. Nakamoto, M. *et al.* Fragile X mental retardation protein deficiency leads to excessive mGluR5-dependent internalization of AMPA receptors. *Proc. Natl Acad. Sci. USA* **104**, 15537–15542 (2007).
55. Wang, H. *et al.* FMRP acts as a key messenger for dopamine modulation in the forebrain. *Neuron* **59**, 634–647 (2008).
56. Park, M., Penick, E. C., Edwards, J. G., Kauer, J. A. & Ehlers, M. D. Recycling endosomes supply AMPA receptors for LTP. *Science* **305**, 1972–1875 (2004).
57. Correia, S. S. *et al.* Motor protein-dependent transport of AMPA receptors into spines during long-term potentiation. *Nature Neurosci.* **11**, 457–466 (2008).
58. Margeta, M. A., Wang, G. J. & Shen, K. Clathrin adaptor AP-1 complex excludes multiple postsynaptic receptors from axons in *C. elegans*. *Proc. Natl Acad. Sci. USA* **106**, 1632–1637 (2009).

METHODS

Reagents. Antibodies: rabbit polyclonal antibodies against human CYFIP1/PIR121/Sra1 (aa 872–886; 1:1000, western blotting; 1:50 immunofluorescence; 4 µg ml⁻¹ immunoprecipitation), Myc (aa 409–420; Upstate, Lake Placid, NY; 1:1000 western blotting; 1:200 immunofluorescence), Myc (A-14 Santa Cruz; 1:20 cryo-immuno EM), MPR (Waguri et al., 2003; 1:200 immunofluorescence), N-WASP-WASP (C-terminus; ECM Biosciences, Versailles, KY; 1:1000 western blotting), CDC42 (C-terminus, Santa Cruz, Santa-Cruz, CA; 1:1000 western blotting), Cathepsin D (Biodesign, Asbach, Germany; 1:1000 western blotting; 4 µg ml⁻¹ immunoprecipitation), NAP1 (aa 1–16; Sigma-Aldrich; 1:1000 western blotting), Rab11a (C terminus, Zymed, San Francisco, CA; 1:100 immunofluorescence), recombinant β-PIX SH3 domain (Millipore, Temecula, CA; 1:1000 western blotting); mouse monoclonal antibodies against mouse AP-1γ (1:1000 western blotting; 1:200 immunofluorescence; 2 µg ml⁻¹ immunoprecipitation), EEA1 (1:200 immunofluorescence), LAMP-1 (CD107a; 1:200 immunofluorescence), human P21-Arc (aa 10–118) (1:200 immunofluorescence), rat GM130 (1:500 immunofluorescence), rat clathrin heavy chain (1:1000 western blotting; 1:100 immunofluorescence) (BD Biosciences, Franklin Lakes, NJ), human transferrin receptor (clone H68.4, Zymed, San Francisco, CA; 1:1000 western blotting; 1:200 immunofluorescence); Myc (clone 9E10; MPI-CBG Antibody Facility, Dresden, Germany; 1:1000 western blotting; 1:100 immunofluorescence; 4 µg ml⁻¹ immunoprecipitation); green fluorescent protein (Roche Applied Science, Mannheim, Germany; 1:100 immunofluorescence), RAC1 (Cell Biolabs, San Diego, CA; 1:1000 western blotting; 1:200 immunofluorescence); rat beta-tubulin (cl. 2.1, Sigma-Aldrich; 1:1000 western blotting; 1:200 immunofluorescence); mouse monoclonal AP-1γ (clone 100/3, Sigma-Aldrich; 1:200 cryo-immuno EM); sheep polyclonal anti-human rTGN46 (GeneTex, San Antonio, TX; 1:200 immunofluorescence).

Secondary antibodies: Alexa Fluor 488, 546 or 647-conjugated against the corresponding primary antibodies (1:400 immunofluorescence) (Molecular Probes, Invitrogen, Germany); horse-radish peroxidase (HRP)-conjugated goat anti-mouse IgG (1:2000 western blotting) and goat anti-rabbit IgG (1:5000 western blotting) (Jackson ImmunoResearch Laboratories, UK).

Latrunculin B, NSC23766 RAC1 inhibitor and D-Mannose-6-Phosphate (M6P) Disodium Salt were from Calbiochem (Germany), and Brefeldin A from Sigma.

Cell culture, transfection and RNA interference. HeLa cells or HeLa cells stably expressing an EGFP-tagged MPR³⁹ were grown in DMEM medium containing 10% fetal calf serum (FCS). Transient expression of Myc-CYFIP2 and GFP-CYFIP1²⁸ was performed with jetPEI (Biomol). BSC1 cells stably expressing EGFP-clathrin light chain or dTomato-clathrin light chain⁵⁹, or EGFP-AP-1σ1 and HEK-293 cells stably expressing GFP-CYFIP1 (ref. 28), EGFP-β-actin or RFP-β-actin were generated as follows. In brief, HEK-293 cells were grown in 24-well plates in DMEM with Glutamax (Gibco) with 10% FCS (Greiner Bio One), and incubated with 1 µg of DNA and 3 µl of jetPEI; after 48 h, 0.8 mg ml⁻¹ Geneticin selective antibiotic (Gibco) was added. After 14 days, cells were transferred to 10-cm plates and grown in DMEM containing 10% FCS and 0.5 mg ml⁻¹ Geneticin. Individual colonies were then picked and transferred to 96-well plates (Bio-One; Greiner). In each case, five or six clones were then chosen by using fluorescence microscopy and tested for expression of the protein of interest by western blotting. For gene silencing, they were transferred into fresh medium and incubated for 72 h with 20 nM siRNAs (HeLa cells) or 50 nM siRNAs (EGFP-β-actin-expressing HEK cells) and Interferin transfection reagent (Biomol). Western blotting or qRT PCR was used to evaluate knockdown efficiencies.

siRNA sequences: AP-1 (NM_001030007), ID 147048, 5'-GGAA-GUUAUGUUCGUGAUGTT-3' and 5'-CAUCACGAACAUAACUUCCTG-3'; CYFIP2 (NM_001037333), IDa 134286, 5'-CCUCCUCCAUAUGU-ACCt-3' and 5'-GGUACAUGAUGGAGGAAGGt-3'; Idb* 134287, 5'-GGUACAUGAGCAGGCUACt-3' and 5'-GUAGCCUGCUCAAUGUACt-3'; CYFIP1 (NM_014608, NM_001033028), IDa 21718, 5'-GGAAUUCAAAGAGUAAGt-3' and 5'-UGCAUUCUGAUCGUAACCGt-3'; Idb* 284749, 5'-CCAAUUU-GUUACAAGCUAtt-3', 5'-CUUAUCUCUUUGAAAUUCct-3'; WAVE2 (NM_006990), ID 138209, 5'-GGUAGGAUUAUGAUAGt-3' and 5'-CUAAUGAUCUAAUCCUACt-3'; WASP (WAS, NM_000377), ID 138724, 5'-GCUGAUUAUGGUGCACCCAtt-3' and 5'-UGGG-UGCACCAAUAUCAGCt-3'; N-WASP (WASL, NM_003941) ID s17132,

5'-CGACAGGGUAUCCAACUAAtt-3' and 5'-UUAGUUGGAUAC-CCUGUCGta-3'; Cdc42 (NM_001039802), ID s2765, 5'-UGGUGCUGUU-GGUAACAtt-3' and UGUUUUACCAACAGCACAtt-3'; Rac1 (NM_198829), ID s11713, 5'-GGAAUAAACUUGAUCUUAtt-3' and 5'-UAAGAUCAGU-UUAGUUCca-3'; clathrin heavy chain (CLTC; NM_004859), ID* 107566, 5'-GGGUGCCAGAUUAUCAUUtt-3' and 5'-AAUUGAUAAUCUGG-CACCCt-3'. ID 107565, 5'-GGCUCAUACCAUGACUGAUtt-3' and 5'-AUCAGUCAUGGUAUGAGCCt-3'; Abi1 (NM_001012750), ID 137945, 5'-GGCAGAUUCUCGACACAAtt and 5'-UUGUGUCGAGAUU-CUGCCt-3'; Beta-PIX (ARHGFE7, NM_003899), ID 119397, 5'-GCAAAUGC-UCGUACAGUCUtt-3' and 5'-AGACUGUACGAGCAUUUGct-3'.

Other two siRNAs targeting β-PIX (NM_003899) were from Invitrogen (5'-GCAGACCAGUGAGAAGUUA-3' and 5'-CCUUCAUGCGCCUG-GAUA-3'). An asterisk indicates the siRNA used predominantly. These siRNAs and nontargeting controls (siNon) no. 2 and no. 6 were purchased from Ambion, Applied Biosciences.

Quantitative RT PCR. Quantitative RT PCR was performed with the MX400 Multiplex QPCR system (Stratagene) and brilliant SYBR Green QPCR Master Mix.

Primers: CYFIP2, 5'-GCAGGAAGGACTTTGTCTC-3' and 5'-CACTG-GGTGATCCTGTTG-3'; CYFIP1, 5'-CAGGATGGAGAGCGTGT-3' and 5'-GGACTCTAGCATGGTTCTC-3'; WAVE2, 5'-GGACGACTG-GTCCGATTA-3' and 5'-GACTTGGAGGAAGCATTG-3'; WASP, 5'-CTGGACCAAGGAGCATTGT-3' and 5'-GTCATCTCCAGCGAAGT-3'; N-WASP, 5'-ACCTTCAAGAGTCCCAC-3' and 5'-CAACACAGATGG-AGGTGG-3'; GAPDH, 5'-TCACCACCATGGAGAAGGC-3' and 5'-GCTA-AGCAGTTGGTGGTGCA-3'.

Immunoprecipitation. Cos-7 cells or HeLa cells transiently transfected with Myc-CYFIP2 were harvested and lysed in 100 mM NaCl, 2 mM EDTA, 50 mM HEPES pH 7.4, 5 mM MgCl₂, 0.5% Nonidet P40 (NP40), 1 mM phenylmethylsulphonyl fluoride (PMSF) and Complete Mini-protease inhibitor mixture (Roche). Lysates were centrifuged for 15 min at 18,000 g and 4 °C, precleared (1 h) with Protein A-Sepharose beads (GE Healthcare) and then incubated for 1 h or overnight at 4 °C with the indicated antibodies (4 µg ml⁻¹). Protein A-Sepharose beads pre-blocked in 1 mg ml⁻¹ BSA were then added to the lysates for 1 h at 4 °C. Beads were recovered by centrifugation, washed either with buffer 1 (150 mM NaCl, 50 mM HEPES pH 7.4, 5 mM MgCl₂, 0.5% NP40, 0.25% Triton X-100, 1 mM PMSF and protease inhibitor cocktail) or with buffer 1 plus 0.5 M Tris-HCl pH 7.4, and resuspended in Laemmli buffer; immunoprecipitates were analysed by SDS-PAGE followed by western blotting. For immunoprecipitation of cathepsin D, HeLa cells were labelled with [³⁵S]methionine and processed as described previously⁶⁰.

Subcellular fractionation. HeLa cells grown in 10-cm plates were washed with PBS, collected in a lysis buffer (100 mM sodium phosphate, 50 mM NaCl, 1 mM MgCl₂, 1 mM EGTA pH 7.4, with protease inhibitor mixture) and passed 15 times through a 27-gauge needle on ice. The lysates were centrifuged for 5 min at 1,000g, and the post-nuclear supernatants were centrifuged for 1 h at 100,000g (Optima Ultracentrifuge, TLA55 rotor; Beckman Coulter) at 4 °C. The membrane pellets and the cytosolic supernatants (equal protein amounts) were analysed by western blotting. Pig brain cytosol was prepared as described previously⁸. Cytosols of HEK cells expressing various GFP-tagged proteins were prepared as described above for HeLa cells.

Yeast two-hybrid analysis. DNA sequences (from imaGenes) encoding CYFIP2 N terminus (residues 2–623), CYFIP2 C terminus (residues 675–1299), clathrin heavy chain N-terminus (residues 1–690), clathrin heavy chain C terminus (residues 821–1679) and NAP1 were subcloned into pGADT7 and pGBKT7 plasmids (Clontech) with the use of restriction endonucleases (Fermentas) to create GAL4 DNA-activation and DNA-binding domain fusions, respectively. The recombinant plasmids were analysed by DNA sequencing. *Saccharomyces cerevisiae* strain AH109 (Clontech) was used for transformations. Yeast transformants were selected on medium SDA –Leu –Trp (MP Biomedicals, LLC). To monitor protein–protein interactions, a selective medium SDA –Ade –Lys –Leu –Trp was used. As negative controls, yeast cells transformed either with the original yeast two-hybrid vectors or with pGBKT7-Lam (Clontech) were used. As positive controls, interaction between SV40 large T-antigen and murine p53, and also known protein interactions, were used.

Cell imaging. Cells were washed with PBS, fixed with 3% paraformaldehyde (PFA) (15 min, 21–24°C), permeabilized with 0.1% Triton X-100 (5 min, room temperature), blocked with 3% BSA (30 min, room temperature), incubated with the primary antibody (1 h, room temperature) and then with corresponding Alexa Fluor-labelled secondary antibodies (20 min, room temperature). Cells were then washed with PBS and mounted on microscope slides with the use of Mowiol (Calbiochem). For measuring transferrin uptake, cells were starved for 1 h in DMEM with 0.2% BSA, incubated with 25 $\mu\text{g ml}^{-1}$ Alexa Fluor 564-labelled transferrin (Molecular Probes) for the indicated durations, placed on ice, washed with ice-cold PBS, fixed, and analysed by microscopy. For measuring transferrin recycling, cells were starved, incubated with Alexa Fluor 564-labelled transferrin for 1 h at 37 °C and washed with ice-cold PBS, then incubated for the indicated durations with 2.5 mg ml^{-1} unlabelled holotransferrin (Calbiochem) in DMEM containing 0.2% BSA. Cells were next fixed and analysed by fluorescence microscopy. For anti-GFP uptake, GFP-MPR HeLa cells were incubated for 1 h on ice with anti-GFP antibodies, then incubated for 60 min at 37 °C, fixed, permeabilized, and labelled with a secondary antibody to detect the internalized anti-GFP antibody. Samples were analysed by confocal fluorescence microscopy, using a LSM 510 meta (Carl Zeiss Microimaging) and a Leica SP5 inverted microscope (Leica Microsystems) and a 63 \times , 1.4 numerical aperture Plan-Apochromat objective (Carl Zeiss Microimaging). Images were analysed with Adobe Photoshop 7 (Adobe Systems), Volocity 5.2 (Improvision) or ImageJ software (<http://rsb.info.nih.gov/ij/>); for statistical analyses we used ANOVA single factor (Excel).

High-speed time-lapse microscopy was performed with an Axiovert 200 M with temperature, CO₂ and humidity control and a 63 \times , 1.2 numerical aperture water-immersion objective (Carl Zeiss Microimaging). Images were collected every 500 ms for 2–4 min. Image analysis was performed with Metamorph software (MDS).

Electron microscopy. HeLa cells transiently expressing Myc-tagged CYFIP2 were fixed for 2.5 h with 2% PFA in 0.1 M phosphate buffer (0.1 M Na₂HPO₄ plus 0.1 M NaH₂PO₄) pH 7.4. Sections 70 nm thick were cut on an ultramicrotome

(Leica). Thawed cryosections were double labelled with the indicated primary and secondary antibodies conjugated to 10-nm or 15-nm gold particles (Cell Microscopy Center, Utrecht Medical School). Sections were analysed with a Philips CM120 (FEI) electron microscope, and images were acquired with a numeric camera (Keen View; Soft Imaging System).

In vitro reconstitution with model membranes. Liposomes coupled with GpI cytoplasmic domains were prepared as described previously⁶¹. GUVs were grown by electrosweating⁶². In brief, 20–50 μl of liposomes was dried onto ITO-slides (Prazisions Glas & Optik) and GUVs were formed in 330 mM sucrose with alternating current (10 Hz, 1.8 V) for 2 h. Functionalized GUVs labelled with DiI C18 or DiD C18 (Molecular Probes) (12 μg) were then incubated as indicated with pig brain cytosol (13 mg ml^{-1}) supplemented with 20% cytosol (about 5 mg ml^{-1} proteins) from cells stably expressing a fluorescently labelled protein of interest in the presence of GTP- γS and imaged by confocal microscopy. Where indicated, an ATP-regenerating system was added. For the actin polymerization assay, cytosols of HEK cells stably expressing EGFP-actin were preincubated with the indicated siRNAs for 72 h or with 100 μM NSC23766 Rac1 inhibitor⁶³ for 1 h at 4 °C. In each case 150 μl cytosol (4–5 mg ml^{-1} protein concentration) and 15 μl DiI C₁₈-labelled GUVs were incubated for 20 min at 37 °C and then imaged with an LSM 510 meta microscope with a 40 \times 1.2 numerical aperture water-immersion objective (Carl Zeiss Microimaging).

59. Ehrlich, M. *et al.* Endocytosis by random initiation and stabilization of clathrin-coated pits. *Cell* **118**, 591–605 (2004).
60. Ludwig, T. *et al.* Differential sorting of lysosomal enzymes in mannose 6-phosphate receptor-deficient fibroblasts. *EMBO J.* **13**, 3430–3437 (1994).
61. Baust, T. *et al.* Protein networks supporting AP-3 function in targeting lysosomal membrane proteins. *Mol. Biol. Cell* **19**, 1942–1951 (2008).
62. Bacia, K., Schuette, C. G., Kahya, N., Jahn, R. & Schwallie, P. SNAREs prefer liquid-disordered over 'raft' (liquid-ordered) domains when reconstituted into giant unilamellar vesicles. *J. Biol. Chem.* **279**, 37951–37955 (2004).
63. Gao, Y., Dickerson, J. B., Guo, F., Zheng, J. & Zheng, Y. Rational design and characterization of a Rac GTPase-specific small molecule inhibitor. *Proc. Natl Acad. Sci. USA* **101**, 7618–7623 (2004).

DOI: 10.1038/ncb2034

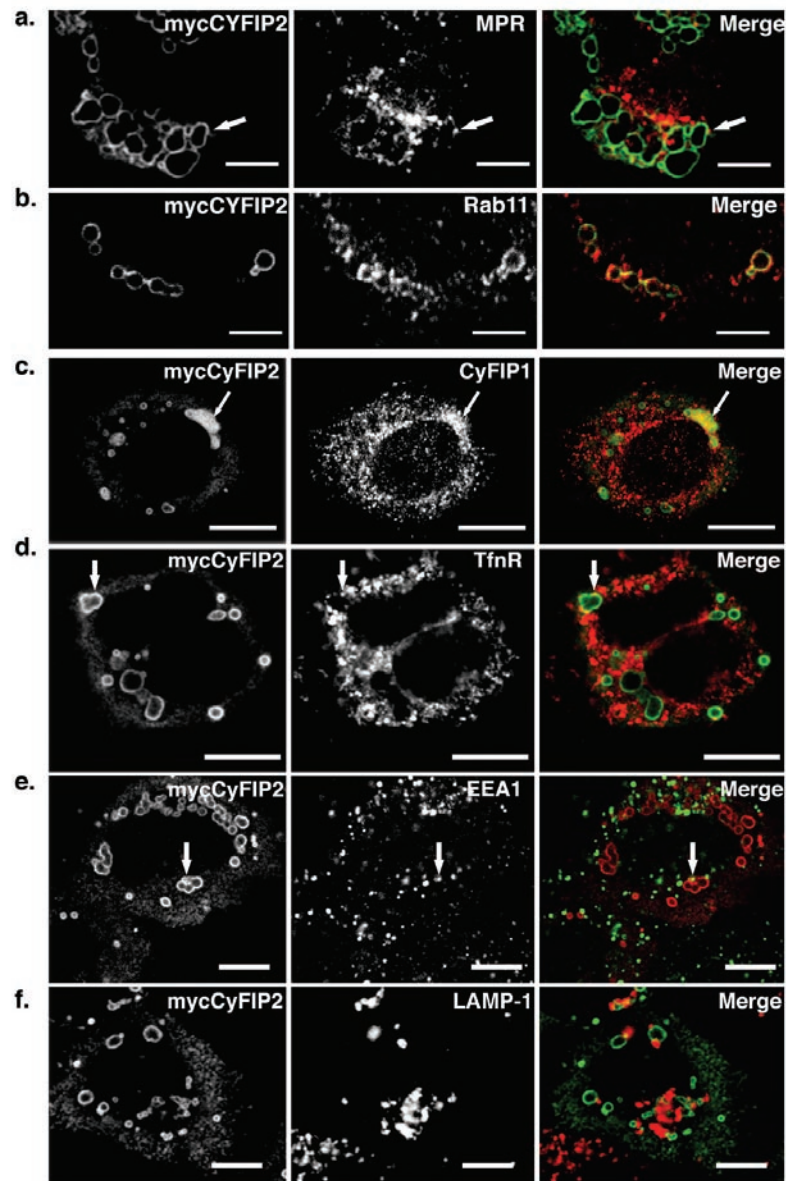
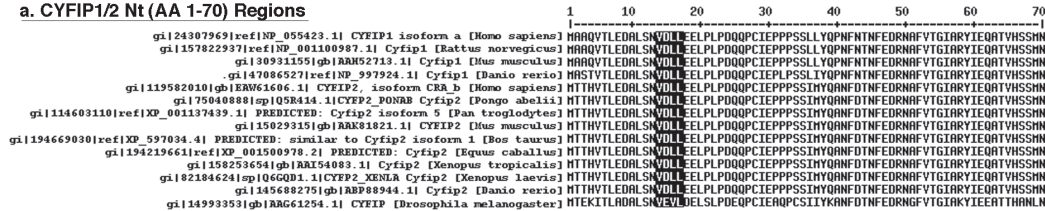


Figure S1 Characterization of the enlarged structures triggered by myc-tagged CYFIP2 expression. HeLa cells expressing myc-tagged CYFIP2 were co-labeled with anti-myc antibodies and antibodies against (a) MPR (red),

(b) Rab11 (red), (c) CYFIP1 (red), (d) TfnR (red), (e) EEA1 (green) or (f) LAMP-1 (red) and analyzed by confocal fluorescence microscopy ($n = 2$ independent experiments). Scale bars, 10 μm .

a. CYFIP1/2 Nt (AA 1-70) Regions



b. CYFIP1/2 Ct (last 285 AA) Regions

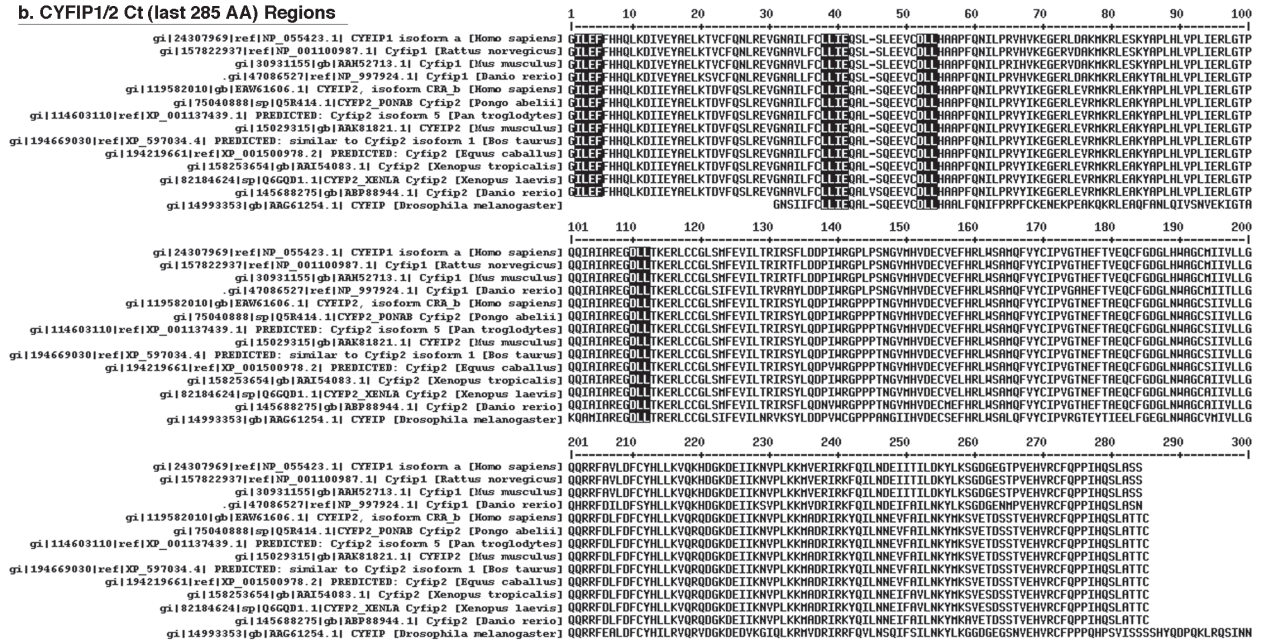


Figure S2 Sequence alignment of the N-terminal (AA 1-70) and the C-terminal (last 285 AA) regions of CYFIP1 and CYFIP2 was done using the

GenBank protein database (<http://www.ncbi.nlm.nih.gov/sites/entrez?db=Protein&itool=toolbar>) and the MultAlin Software¹.

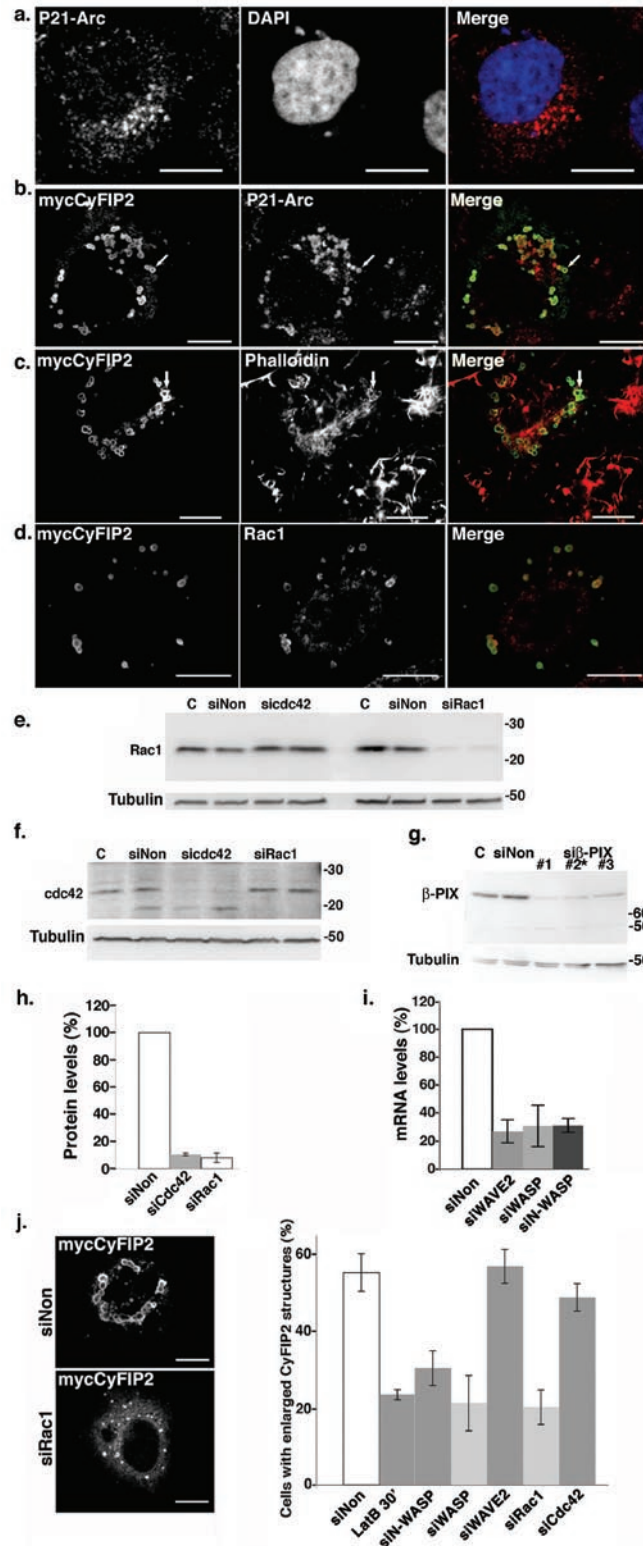


Figure S3 N-WASP/WASP and RAC1 act together with CYFIP during actin nucleation on membranes. **(a)** Mock transfected or **(b-d)** myc-CYFIP2 expressing HeLa cells were labeled with anti-myc (green) and **(a, b)** anti-P21Arc (red), **(c)** Alexa 594-labeled phalloidin (red), or **(d)** anti-RAC1. **(e-h)** The efficiencies of the siRNA mediated knockdowns of RAC1, CDC42 and β -PIX were analyzed by western blotting, quantified and normalized to tubulin levels. **(i)** Efficiencies of the WAVE2, WASP and N-WASP knockdowns were evaluated by Q RT-PCR and mRNA levels were normalized

to GAPDH ($n = 3$ independent experiments; data represent the mean \pm s.d.). **(j)** HeLa cells were transfected with the indicated siRNAs, and after 1 day transfected with myc-CYFIP2. After 2 more days, cells were fixed, labeled with anti-myc and analyzed by confocal fluorescence microscopy. The percentages of cells displaying enlarged vacuoles due to CYFIP2 expression were quantified using Anova single factor ($n > 500$ cells, $n = 3$ independent experiments in duplicate; data represent the mean \pm s.d.; $p < 0.0001$, $\alpha = 0.05$). Scale bars, 10 μ m.

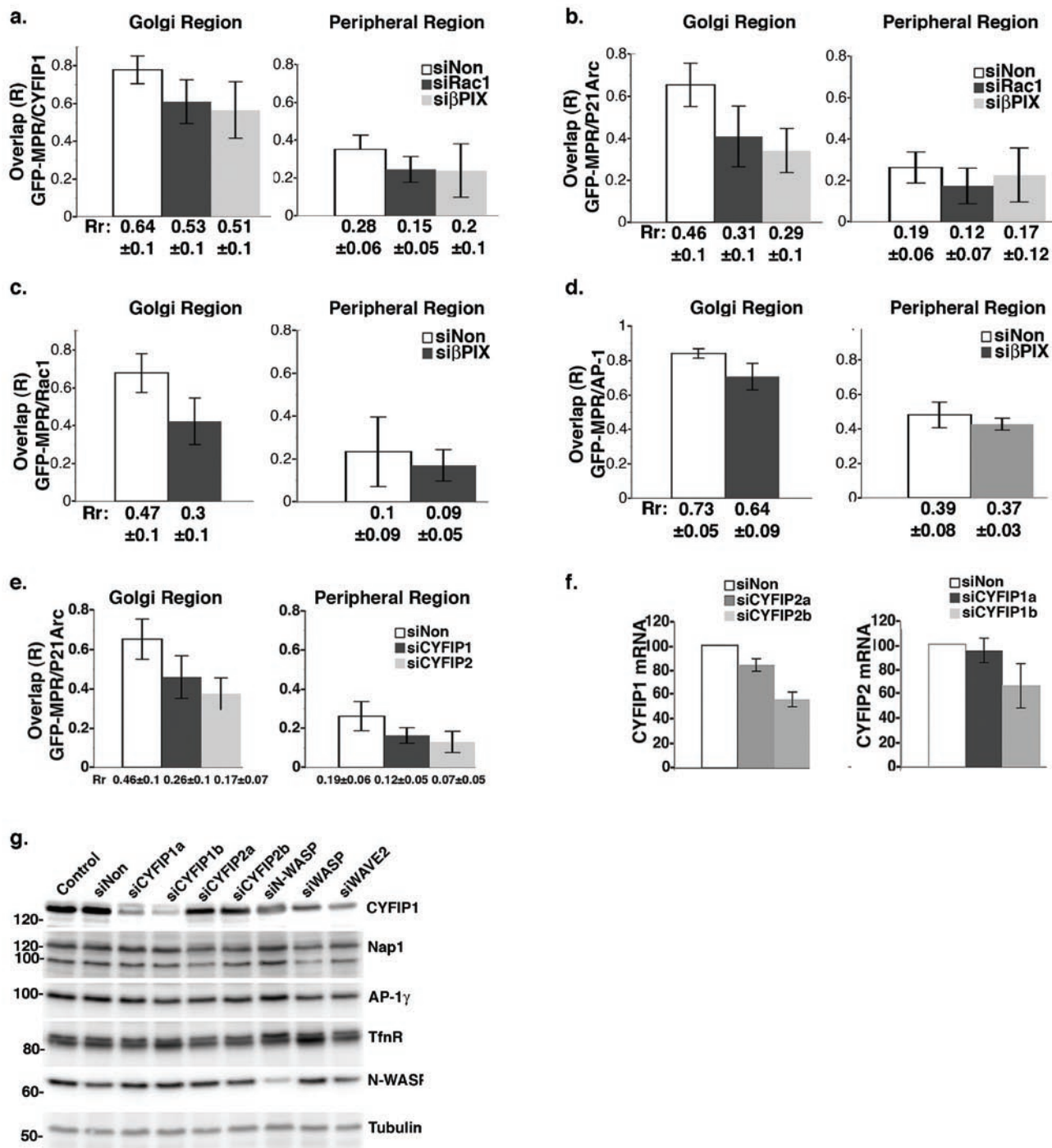


Figure S4 Co-localization quantification and siRNA-mediated knock-down efficiency analysis. **(a-e)** Co-localization in the Golgi and peripheral regions between **(a)** GFP-MPR and CYFIP1, **(b, e)** GFP-MPR and P21-Arc, **(c)** GFP-MPR and RAC1, **(d)** GFP-MPR and AP-1γ was analyzed and quantified with Velocity 5.2 software. R = overlap coefficients, Rr = Pearson correlation coefficients. More than 20 representative cells (n = 3 independent experiments) were analyzed per condition; data represent the mean ± s.d.

(f) The levels of CYFIP1 mRNAs following the knock-down of CYFIP2, and of CYFIP2 mRNAs following the knock-down of CYFIP1 were measured by Q RT-PCR; GAPDH was used as a control (n = 4 independent experiments; data represent the mean ± s.d.). **(g)** Protein levels of CYFIP1, NAP1, AP-1γ, TfnR, N-WASP and tubulin were analyzed by western blotting after the indicated knockdowns (images are representative of n = 3 independent experiments, n = 5 independent experiments for anti-CYFIP1 and anti-tubulin).

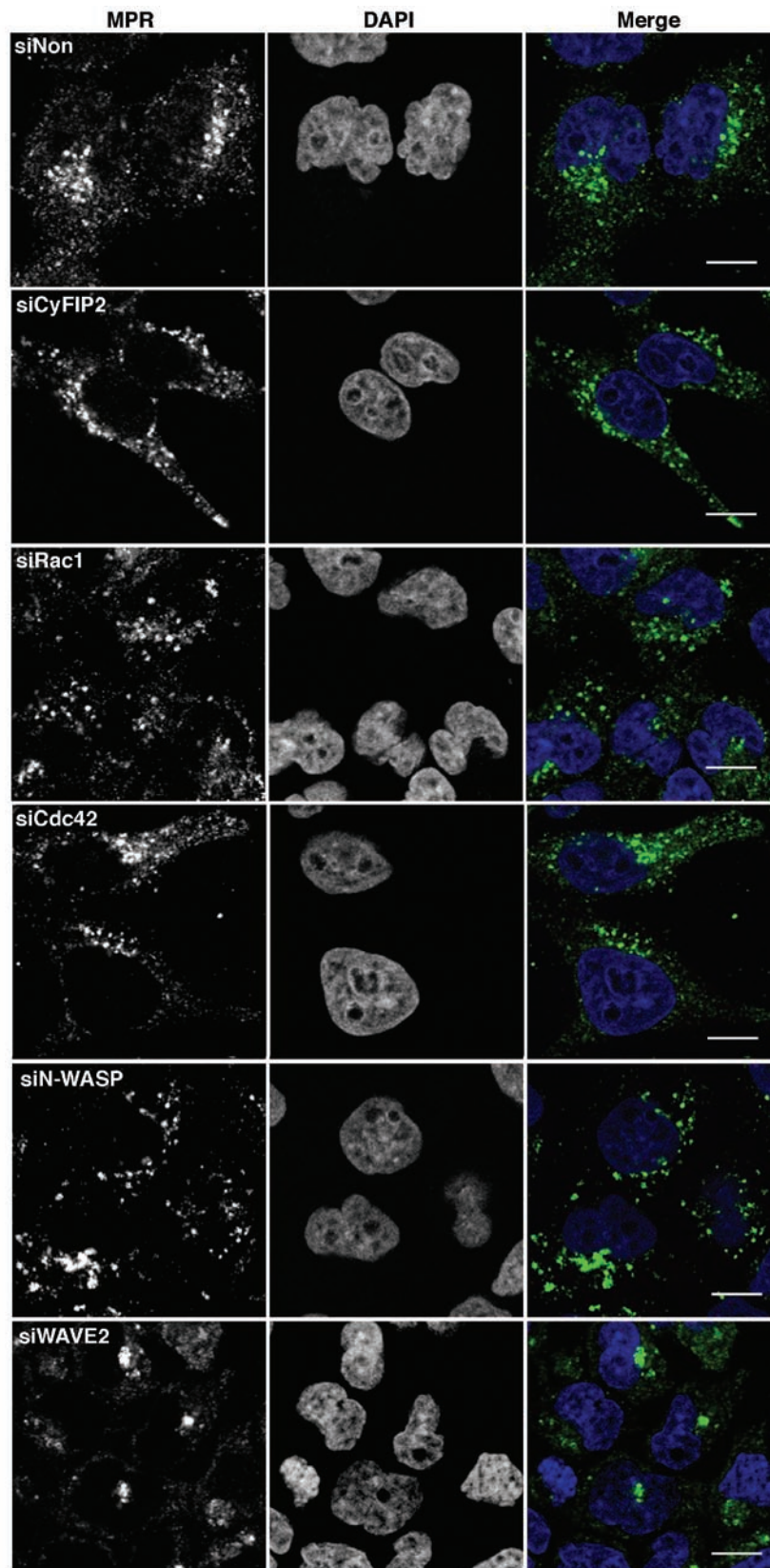


Figure S5 Morphology of the endogenous MPR-rich compartments in siRNA treated cells. HeLa cells were transfected with the indicated

siRNAs for 72 h, then labeled with anti-MPR (green) and DAPI (blue). Scale bars, 10 μ m.

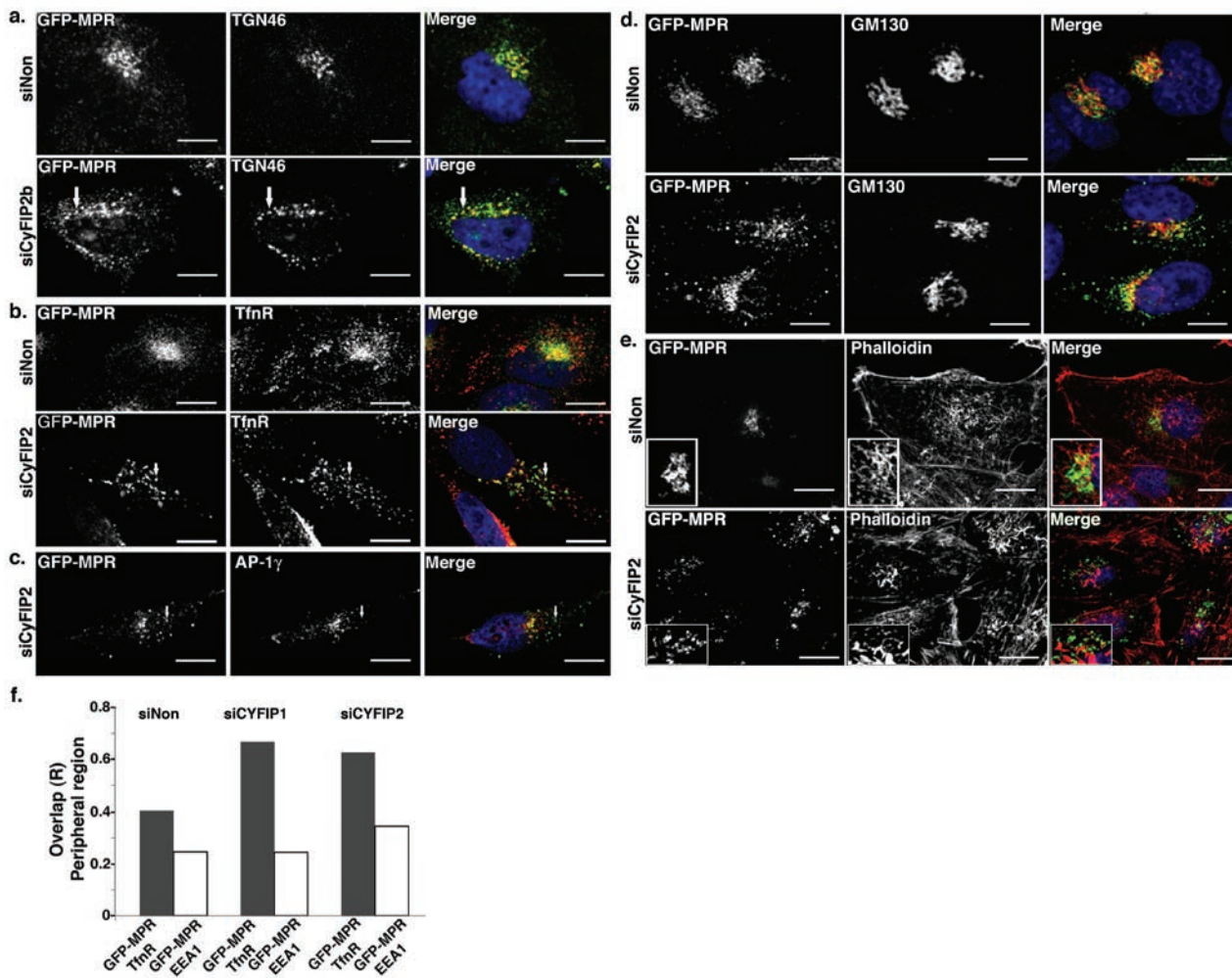


Figure S6 CYFIP2 depletion results in the fragmentation of the TGN/recycling endosomes. GFP-MPR expressing HeLa cells were transfected with control siRNAs or with siRNAs targeting CYFIP2 for 72 h. Cells were fixed and then labeled with antibodies against (a) TGN-46, (b) Tfnr, (c) AP-1 γ , (d) GM-130 or (e) with Alexa Fluor 546-phalloidin

and analyzed by confocal fluorescence microscopy. (f) Co-localization between peripheral GFP-MPR and Tfnr or EEA1 was calculated for each of the indicated conditions. More than 20 representative cells from $n = 2$ independent experiments were analyzed per condition. Scale bars, 10 μ m.

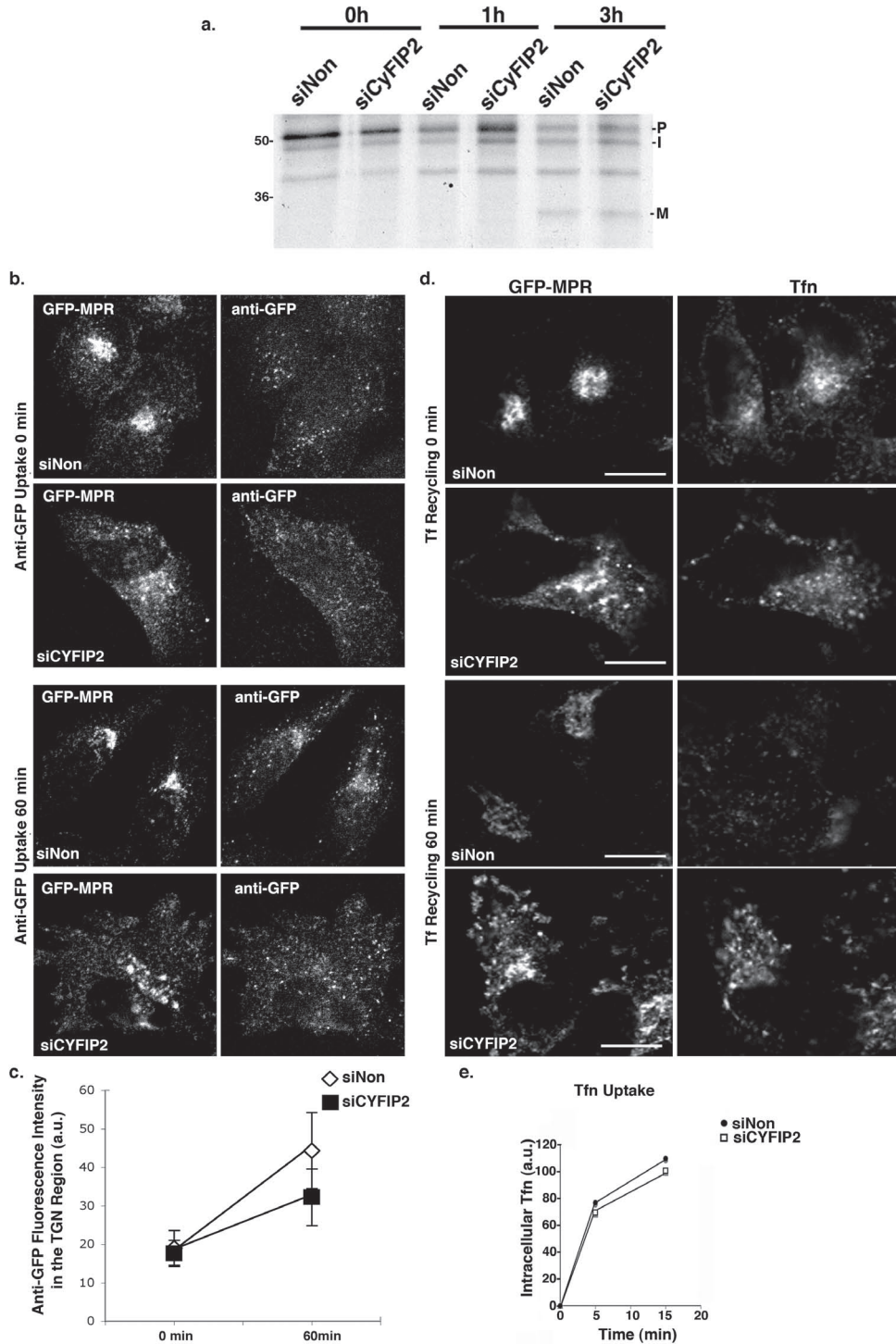


Figure S7 Effect of CYFIP2 knock-down on cargo trafficking. **(a)** HeLa cells were labeled with ^{35}S Methionine for 30 min, then pulse-chased for the indicated times. Cathepsin D was immunoprecipitated from the lysates and analyzed by SDS-PAGE. The relative levels of the precursor (P), intermediate (I) and mature (M) forms were quantified relative to the total Cathepsin D levels. **(b, c)** GFP-MPR expressing HeLa cells transfected with the indicated siRNAs for 72 h were labeled with anti-GFP antibodies at 4°C, chased for 60 min at 37°C, fixed and stained with a secondary antibody. **(c)** Fluorescence intensities of anti-GFP detected in the perinuclear (TGN) region were

quantified ($n = 50$ cells; data represent the mean \pm s.d.). **(d, e)** GFP-MPR expressing HeLa cells transfected with the indicated siRNAs for 72 h were incubated with Alexa Fluor 564-labeled Tfn. **(d)** For the recycling assay, cells were chased in the presence of unlabeled Tfn for the indicated times. **(e)** For Tfn uptake quantification cells were starved for 1 h and incubated with fluorescent-labeled Tfn at 37°C for the indicated periods of time ($n = 2$ independent experiments in duplicate). The amount of intracellular fluorescent Tfn was measured by fluorescence microscopy and quantified using ImageJ. Scale bars, 10 μm .

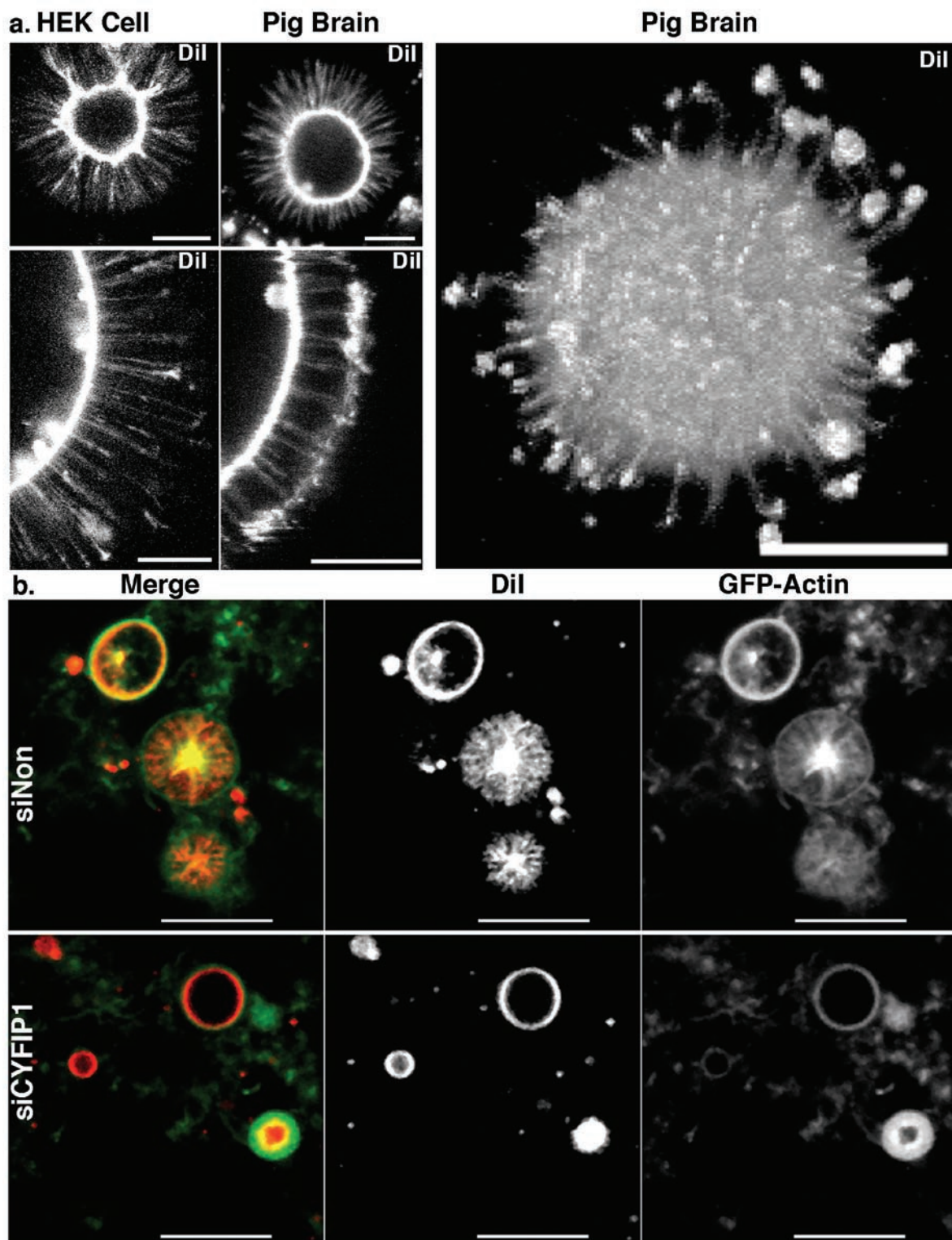


Figure S8 Formation of membrane tubules from GUVs. (a) Dil C18-labeled GUVs with Gpl tails and PI-4P were incubated in the presence of an ATP regenerating system either with HEK cell cytosol or with pig brain cytosol as indicated. The upper right panel shows a 3D reconstruction of a GUV

incubated with pig brain cytosol. (b) Dil C18-labeled GUVs with Gpl tails and PI-4P were incubated with an ATP regenerating system and with cytosol of GFP-Actin expressing HEK cells treated with the indicated siRNAs. Scale bars, (a) 10 μ m and (b) 20 μ m.

Fig. 2e

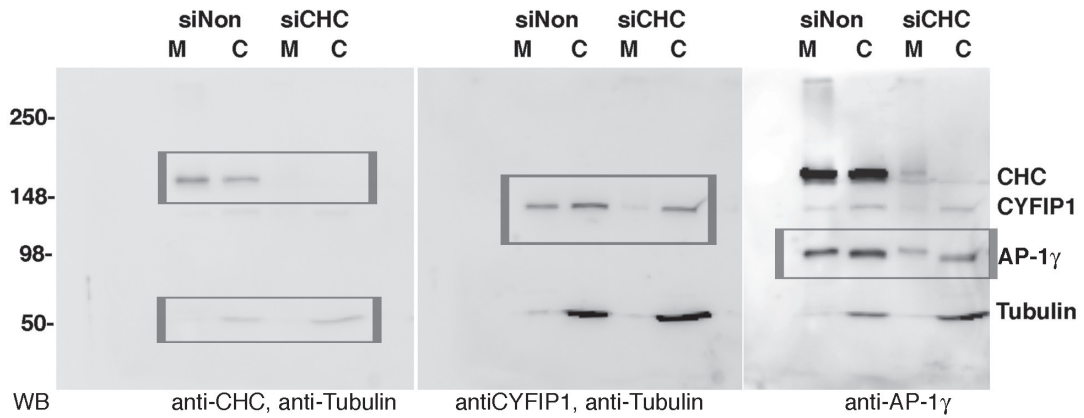


Fig. 2f

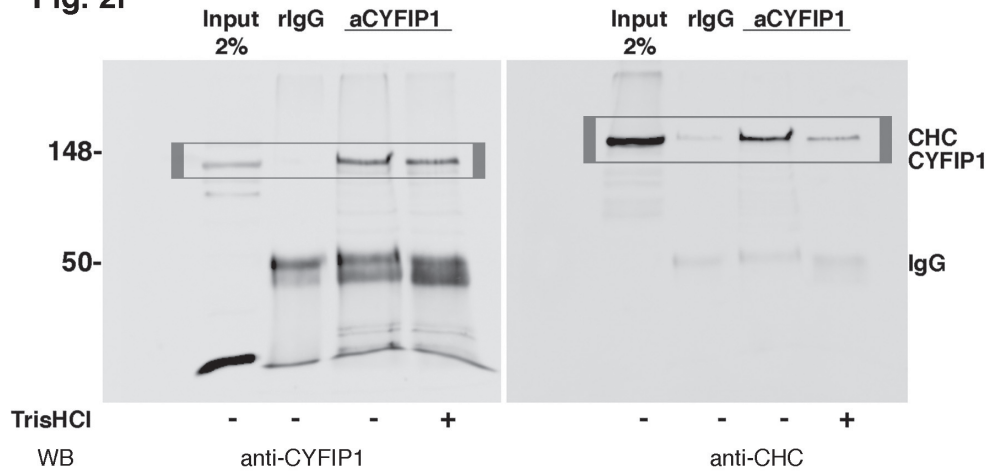


Fig. 2g

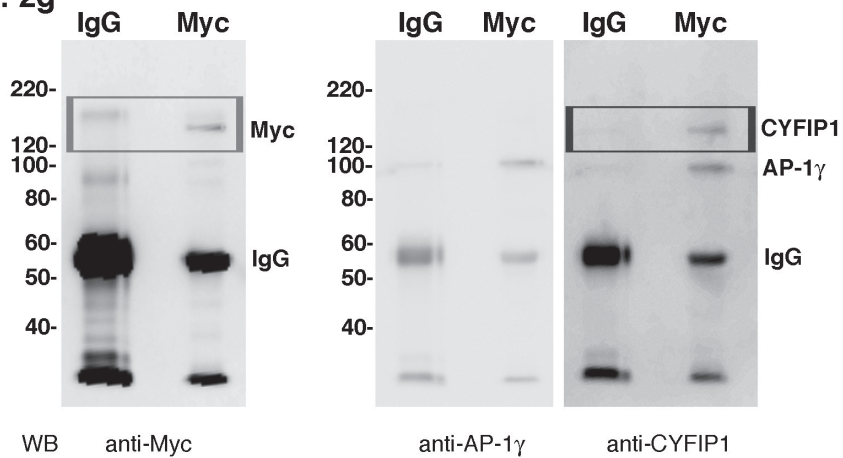


Figure S9 Uncropped image blots

Supplementary Movies 1, 2, 4-9. GFP-MPR dynamics in HeLa cells. GFP-MPR expressing HeLa cells were transfected with (1) control siNon, (2) siCYFIP2, (4) siCYFIP1, (5) siN-WASP, (6) siRAC1, (7) si β -PIX or (8) siCDC42 siRNAs for 72 h, or (9) 100 μ M RAC1 inhibitor (NCS 23766) for 1.5-2 h. The number of GFP-MPR positive tubules exiting from the TGN region was analyzed using time-lapse fluorescence microscopy as indicated in Table 1. The interval between the acquisition of two consecutive images is $t = 500$ ms, and the total acquisition time is (1, 4-9) $T = 4$ min or (2) $T = 2$ min.

Supplementary Movie 3 Tubule formation on model membranes induced by actin polymerization. Dil C18 labeled GUVs with PI-4P and Gpl cytoplasmic domains were incubated at 37°C with pig brain cytosol in the presence of an ATP regenerating system, and imaged by time-lapse videomicroscopy. Images were captured every $t = 1$ min during $T = 30$ min.

1. Corpet, F. Multiple sequence alignment with hierarchical clustering. *Nucleic Acids Res* **16**, 10881-90 (1988).